Master's thesis

NTNU
Norwegian University of Science and Technology
Faculty of Natural Sciences
Department of Materials Science and Engineering

Alexander Svalheim Lien

Hybrid epoxy nanocomposites for high voltage application

Master's thesis in Materials Science and Technology
Supervisor: Mari-Ann Einarsrud
Co-supervisor: Mohammed Mostafa Adnan
July 2022

NTNU
Norwegian University of
Science and Technology

Alexander Svalheim Lien

Hybrid epoxy nanocomposites for high voltage application

Master's thesis in Materials Science and Technology
Supervisor: Mari-Ann Einarsrud
Co-supervisor: Mohammed Mostafa Adnan
July 2022

Norwegian University of Science and Technology
Faculty of Natural Sciences
Department of Materials Science and Engineering

NTNU
Norwegian University of
Science and Technology

Declaration

I hereby declare that the work presented in this document has been performed independently and in accordance with the rules and regulation of the Norwegian University of Science and Technology (NTNU).

Trondheim, July 2022

Alexander Svalheim Lien

Acknowledgements

First of all I would like thank my supervisor, Professor Mari-Ann Einarsrud, for giving me motivation and guidance during my final year of my study program. I would also like to thank my friends at the university and my family at home for their support and encouragement during my master's program. Lastly, I thank the technical staff at the department for helping me with equipment training that I needed to use in my master's thesis and NTNU Nanolab for letting me use their equipment in their cleanroom.

Abstract

Hybrid epoxy nanocomposites with TiO_2 or Al_2O_3 nanoparticles as filler have proven to have excellent dielectric properties which can be utilized in high voltage insulation applications. Epoxy nanocomposites can be synthesized by either the ex situ method, where the inorganic nanoparticles are pre-synthesized and mechanically mixed with the epoxy monomer, or the in situ method, where the inorganic nanoparticles are grown and nucleated within the epoxy matrix. Traditionally, producing hybrid epoxy nanocomposites by the ex situ method is done by mechanically mixing the nanoparticles with the highly viscous epoxy monomer. In this work, the ex situ synthesis method was adapted by first mixing the nanoparticles with the curing agent and then mixing the curing agent dispersion with the epoxy monomer. The reason for this is that the curing agent is much less viscous than the epoxy. Ex situ synthesized epoxy nanocomposites often have the inorganic nanoparticles agglomerated in the epoxy matrix as dispersion is a challenge. Surface functionalization by (3-aminopropyl)triethoxysilane (APTES) was performed on as-received TiO_2 and Al_2O_3 nanoparticles to reduce agglomeration of the nanoparticles and to increase the dispersion of the nanoparticles in the epoxy polymer.

A qualitative analysis by Fourier transform infrared- and Raman spectroscopy showed that the functionalization of the nanoparticles was successful by the presence of characteristic bands from APTES. Thermogravimetric analysis revealed that APTES surface coverage of functionalized TiO_2 and Al_2O_3 was 30.9 % and 43.1 % respectively. Nanoscale imaging showed that agglomerates had formed in the epoxy nanocomposites ranging from 30 nm up to 1 μm in size and low magnification images revealed that the agglomerates were not well-dispersed in the epoxy with free path lengths up to 800 nm. However, the epoxy nanocomposites with functionalized nanoparticles generally were more well-dispersed and had smaller agglomerates on average compared to epoxy nanocomposites with as-received nanoparticles. This shows that functionalizing the nanoparticles had a positive effect with respect to agglomerate size and dispersion of the epoxy nanocomposites. Impedance spectroscopy showed that the dielectric properties of the pure epoxy was generally better than epoxy nanocomposites. However, some of the epoxy nanocomposites at low filler content exhibited desirable dielectric properties with lower permittivity and dielectric loss than pure epoxy. Furthermore, epoxy nanocomposites with functionalized oxide nanoparticles generally had lower permittivity compared to epoxy nanocomposites synthesized with as-received oxide nanoparticles. Differential scanning calorimetry revealed that incorporation of oxide nanoparticles at low filler content resulted in a decrease in the glass transition temperature, T_g, compared to pure epoxy and that T_g increased with increasing filler content in the epoxy nanocomposites. Additionally, epoxy nanocomposites synthesized with functionalized oxide nanoparticles had a higher T_g compared to their as-received counterparts.

Sammendrag

Hybrid epoksy nanokompositter med uorganiske TiO_2 eller Al_2O_3 nanopartikler som fyllmateriale har vist seg å ha utmerkede dielektriske egenskaper og kan bli brukt som isolasjon i høyspenningsapplikasjoner. Epoksy nanokompositter kan bli syntetisert enten med ex situ methoden, der de uorganiske nanopartiklene er syntetisert på forhånd og mekanisk blandet med epoksy monomeren, eller in situ metoden, der de uorganiske nanopartiklene gror og nukleeres inni epoksy matriksen. Hybrid epoksy nanokompositter som blir produsert med ex situ metoden er vanligvis gjort ved å blande nanopartiklene med den viskøse epoksy monomeren. I dette arbeidet, ex situ syntesemetoden var adaptert ved å først blande nanopartiklene med herdemiddelet og deretter blande herdemiddelløsningen med epoksy monomeren. Nanopartiklene i epoksy nanokompositter syntetisert med ex situ metoden agglomererer ofte så spredningen av nanopartiklene er en utfordring. TiO_2 og Al_2O_3 nanopartikler ble overflatefunksjonalisert med (3-aminopropyl)triethoxysilane (APTES) for å redusere agglomerasjon og øke spredningen av nanopartiklene i epoksy polymeren.

En kvalitativ analyse var utført med Fourier transform infrarød spektroskopi og Raman spektroskopi som viste at funksjonaliseringen av nanopartiklene var vellykket ved observasjon av karakteristiske bånd som kun finnes i APTES. Termogravimetrisk analyse viste at overflatedekningen av APTES på TiO_2 og Al_2O_3 nanopartiklene var henholdsvis 30.9 og 43.1 %. Avbildning av epoksy nanokomposittene på nanoskala viste at agglomerater hadde blitt dannet, og at de hadde størrelser fra 30 nm til 1 μm. Bilder med lav forstørrelse viste at agglomeratene ikke hadde god spredning i epoksy polymeren med frie veilengder opp til 800 nm. Imidlertid, epoksy nanokomposittene med funksjonaliserte nanopartikler hadde generelt bedre spredning og mindre agglomerater enn epoksy nanokompositter med ufunkasjonaliserte nanopartikler. Dette betyr at funksjonalisering av nanopartiklene hadde en positiv effekt med tanke på agglomeratstørrelse og spredning i epoksy nanokomposittene. Impedansspektroskopi viste at de dielektriske egenskapene av ren epoksy var generelt bedre enn epoksy nanokomposittene. Noen av epoksy nanokomposittene med lav fyllmengde hadde derimot ønskede dieletriske egenskaper med lavere relativ permittivitet og dielektrisk tap i forhold til ren epoksy. I tillegg, epoksy nanokompositter med funksjonaliserte nanopartikler hadde generelt lavere permittivitet sammenliknet med epoksy nanokompositter som ble syntetisert med ufunksjonaliserte nanopartikler. Differensiell skanning kalorimetri viste at inkorporering av nanopartikler ved lave fyllmengder resulterte i en reduksjon av glassovergangstemperaturen, T_g, sammenliknet med ren epoksy og at T_g økte med en økning av fyllmengden i epoksy nanokomposittene. I tillegg, epoksy nanokompositter syntetisert med funksjonaliserte nanopartikler hadde høyere T_g sammenliknet med epoksy nanokompositter med ufunksjonaliserte nanopartikler.

Contents

1 Background **13**

1.1 Motivation 13

1.2 Aim and scope of work 15

2 Introduction **17**

2.1 Nanocomposite materials 17

2.1.1 Epoxy-based nanocomposites 17

2.1.2 SiO_2, TiO_2 and Al_2O_3 epoxy nanocomposites 20

2.2 Dielectrics and dielectric properties 26

2.2.1 Dielectric materials 26

2.2.2 Complex permittivity 26

2.3 Thermal properties 27

3 Experimental **29**

3.1 List of chemicals 29

3.2 Surface functonalization 29

3.3 Ex situ nanocomposite synthesis 29

3.4 Characterization 30

3.4.1 Fourier transform infrared spectroscopy 30

3.4.2 Thermogravimetric analysis 31

3.4.3 Impedance spectroscopy 31

3.4.4 Surface area measurements 31

3.4.5 Scanning (transmission) electron microscopy 32

3.4.6 Differential scanning calorimetry 32

3.4.7 Raman Spectroscopy 32

4 Results **33**

4.1 Characterization of surface functionalized nanoparticles 33

4.1.1 Fourier transform infrared spectroscopy 33

4.1.2 Raman Spectroscopy 35
4.1.3 Surface area measurement and thermogravimetric analysis . . . 37
4.2 Characterization of hybrid epoxy nanocomposites 39
4.2.1 Impedance spectroscopy 39
4.3 Nanoscale imaging 41
4.4 Glass transition temperature 44

5 Discussion **47**
5.1 Functionalization of as-received TiO_2 and Al_2O_3 nanoparticles 47
5.2 Synthesis procedure of functionalized TiO_2 and Al_2O_3 epoxy nanocomposites 47
5.3 Electrical properties 49
5.4 Thermal properties 51

6 Conclusion **53**

7 Further work **55**

List of abbreviations

SCAs	Silane coupling agents
APTES	(3-aminopropyl)triethoxysilane
DGEBA	Diglycidyl ether of bisphenol-A
TGA	Thermogravimetric analysis
BET	Brunauer–Emmett–Teller
S(T)EM	Scanning (Transmission) electron microscopy
FTIR	Fourier Transform Infrared Spectroscopy
DSC	Differential scanning calorimetry
T_g	Glass transition temperature

1 Background

1.1 Motivation

The field of dielectrics was introduced in the mid-1800s when Michael Faraday studied the insulation properties of materials. A material which is electrically insulating and has the ability to store electrical charge is called a dielectric. When a dielectric is exposed to an external electric field the positive and negative charged species (dipoles) become polarised and they are displaced in the direction of the electric field. This effect is shown in figure 1.1. The electric field between two charges in a dielectric medium is less than it would have been in vacuum as a result of this [1]. As development and miniaturization of electronic technology continues, there is a constant need for better and more versatile dielectric materials.

Dielectrics are often used as insulators in electrical applications because of their ability to prevent electrons from flowing freely through the material. Good electrical insulators have the ability to withstand high voltages without becoming electrically conductive. The voltage at which an electrical insulator becomes conductive is known as the dielectric breakdown strength [2]. This is an important parameter to consider in high voltage applications as a dielectric breakdown in an electrical system could be detrimental and potentially very harmful.

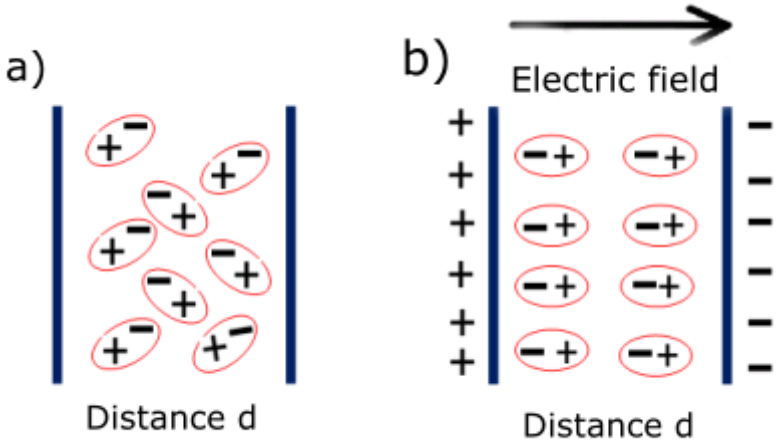

Figure 1.1: Dipoles in a dielectric material when there is a) no external electric field and b) an external electric field applied. The dipoles line up in the direction of the electric field and are displaced with respect to their original location.

Hybrid epoxy nanocomposites have proven to be a solid candidate for high voltage insulation applications. These materials consist of oxide or non-oxide inorganic nanoparticles such as silicon dioxide (SiO_2, titanium oxide (TiO_2) and aluminium nitride (AlN) dispersed in an organic epoxy matrix. Epoxy is a brittle polymer with low dielectric constant [3], and the inorganic filler nanoparticles usually have high relative permittivity, thermal conductivity and mechanical strength. The most commonly used epoxy for hybrid epoxy nanocomposite synthesis is diglycidyl ether of bisphenol-

A (DGEBA) [4]. This dielectric material can be used in nanodielectrics, coatings, catalysts and more [5]–[7]. It may also be suitable as a high voltage insulation material in emerging fields such as electrified aircrafts due to epoxy nanocomposites being light weight while also having the ability to withstand high voltages. Pure epoxy is already widely used as an electrically insulating material in power equipment such as circuit boards, rotating machines and switchgear spacers [4]. The disadvantage of using pure epoxy is that it is brittle and it breaks down at relatively low temperature [8], which would prove detrimental in high voltage insulation applications. The mechanical and thermal properties can be enhanced by introducing inorganic oxide filler microparticles, producing an epoxy-based composite [9]. The enhancement of the mechanical and thermal properties will come at the cost of increased complex permittivity and reduced dielectric breakdown strength [10]. However, replacing the microparticles with nanoparticles may increase the composite's mechanical and thermal properties while also retaining the dielectric properties of the epoxy. The challenge is to find an easy and reproducible synthesis route for these hybrid epoxy nanocomposites with the inorganic oxide filler nanoparticles homogeneously dispersed within the epoxy matrix. As the particles approach the nanometer scale, the relative surface area over volume ratio increases, and so does the surface energy [11]. A consequence of this is that the nanoparticles tend to agglomerate in order to reduce this surface energy, making it difficult to keep the nanoparticles homogeneously dispersed in the epoxy matrix at the nanoscale. This is not desired as the agglomerated particles may approach micrometer size which will reduce the dielectric properties of the composite. A possible solution to this challenge is to modify the surface of the nanoparticles. Surface modification of nanoparticles are often done by using surfactants or coupling agents [12]. Surfactants are long organic molecules with a functional head group and an alkyl chain. The functional head group physically adsorbs on the surface of the nanoparticle preventing it from agglomerating with other particles. These molecules can be used to provide steric hinderance or electric repulsion from other particles which can reduce agglomeration and increase dispersion. Coupling agents function similarly to surfactants, but instead of adsorbing physically, they react chemically to the surface of the particle, making them more strongly bonded with the surface of the particle [13]. These molecules reduce agglomeration by ensuring strong chemical bonds between the organic and inorganic components in the epoxy composite, but they can also provide steric hinderance and electric replusion based on the alkyl chains of the coupling agent.

Two main synthesis routes have been proposed for producing hybrid epoxy nanocomposites reliably with homogeneously dispersed nanoparticles: the traditional ex situ route and the alternative in situ route. Nanocomposites synthesized by the ex situ route are generally made by mechanically mixing the nanoparticles with the epoxy monomer. Due to the high viscosity of the epoxy monomer, it is difficult to homogeneously disperse the nanoparticles. However, it may be an option to mix the nanoparticles with the curing agent instead to improve the homogenity of these particles in the epoxy matrix and still use the ex situ route. In the in situ route, the nanoparticles are nucleated inside the epoxy by adding a molecular precursor of the desired nanoparticle followed by hydrolysis and polycondensation reactions to form inorganic nanoparticles in the epoxy matrix (sol-gel reactions) [14]. Designing a reliable synthesis route for well-dispersed hybrid epoxy nanocomposites could be a significant step

in the technological progress of electrical insulators.

1.2 Aim and scope of work

The scope of the master's thesis was to improve the ex situ synthesis route of hybrid epoxy-based nanocomposites. Aluminium oxide (Al_2O_3) and titanium dioxide (TiO_2) are often used in the literature, and were therefore chosen as the inorganic filler materials for the epoxy nanocomposites. The aim was to create well-dispersed epoxy nanocomposites with desired properties by mixing the inorganic oxide nanoparticles with the curing agent rather than directly mixing them with the viscous epoxy monomer. The first strategy was approached by mixing pure TiO_2 or Al_2O_3 nanoparticles in the curing agent at 1 wt%, 3 wt% and 5 wt% and characterize the dispersion of the particles in the epoxy matrix. The second strategy was to functionalize the oxide nanoparticles with a silane coupling agent before mixing them with the curing agent to increase the degree of dispersity. The surface functionalization was monitored by Fourier transform infrared spectroscopy, Raman spectroscopy, nitrogen adsorption and thermogravimetry to investigate if the surface of the nanoparticles had been functionalized and to which degree. Impedance spectroscopy, differentialy scanning calorimetry and bright field scanning (transmission) electron microscopy were used to characterize the synthesized nanocomposites and see if the properties of the nanocomposites had improved based on the changes in the synthesis route.

2 Introduction

2.1 Nanocomposite materials

A composite material consists two or more individual materials which have different properties when combined together. Composite materials often have more desired properties than the individual materials they are made of. A material is considered a nanocomposite if one or more of the components are within the sub 100 nanometer range [15]. As particles become smaller in size, the volume ratio to surface area decreases, which will change the properties of the material. As such, the properties of the individual components may not necessarily be reflected in the composite material in a 1:1 ratio as interactions between them can have a synergetic effect which results in different properties. Thus, nanocomposites can have unique and multifunctional properties.

2.1.1 Epoxy-based nanocomposites

Epoxy is an organic network polymer where the monomers are cross-linked with covalent bonds. Epoxy is a thermosetting polymer, which means it becomes permanently hard upon curing [16]. Therefore, epoxy is mechanically stronger than most thermoplastics, but this also means that it is a brittle material. The most commonly used epoxy for electrical insulation research is called diglycidyl ether of bisphenol-A (DGEBA) and it is used due to its outstanding dielectric properties. A DGEBA monomer is formed when Bisphenol-A reacts with the epoxide diglycidyl. The monomer further reacts with a curing agent to produce a hybrid molecule which then reacts with an additional DGEBA monomer which starts the cross-linking process. The final product is a cross-linked epoxy polymer [17]. The figures 2.1 to 2.3 shows an illustration of the polymerization process of DGEBA.

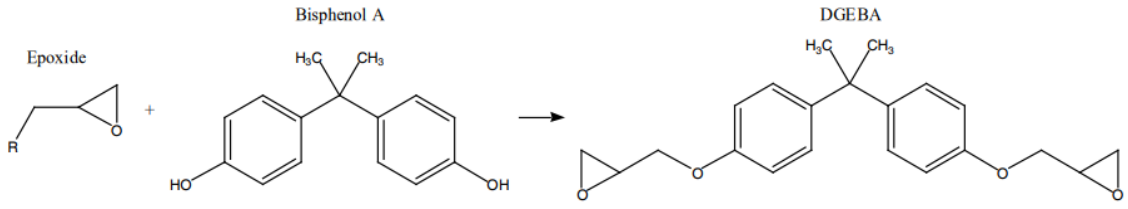

Figure 2.1: Reaction between the epoxide diglycidyl ether and Bisphenol-A to produce a DGEBA monomer. Adapted from F. Zaragoza et al. [17].

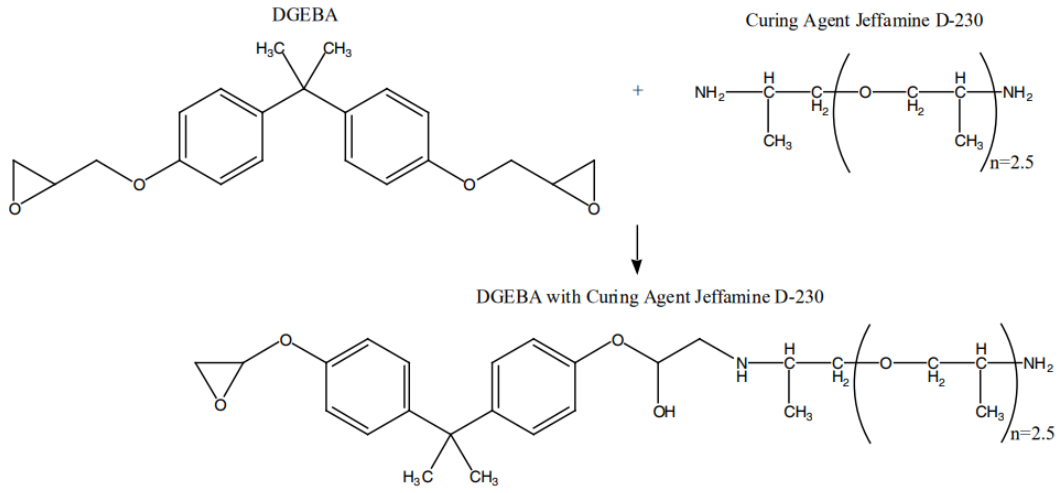

Figure 2.2: Reaction between a DGEBA monomer and the curing agent Jeffamine D-230 to produce a DGEBA-Jeffamine D-230 hybrid molecule. Adapted from F. Zaragoza et al. [17].

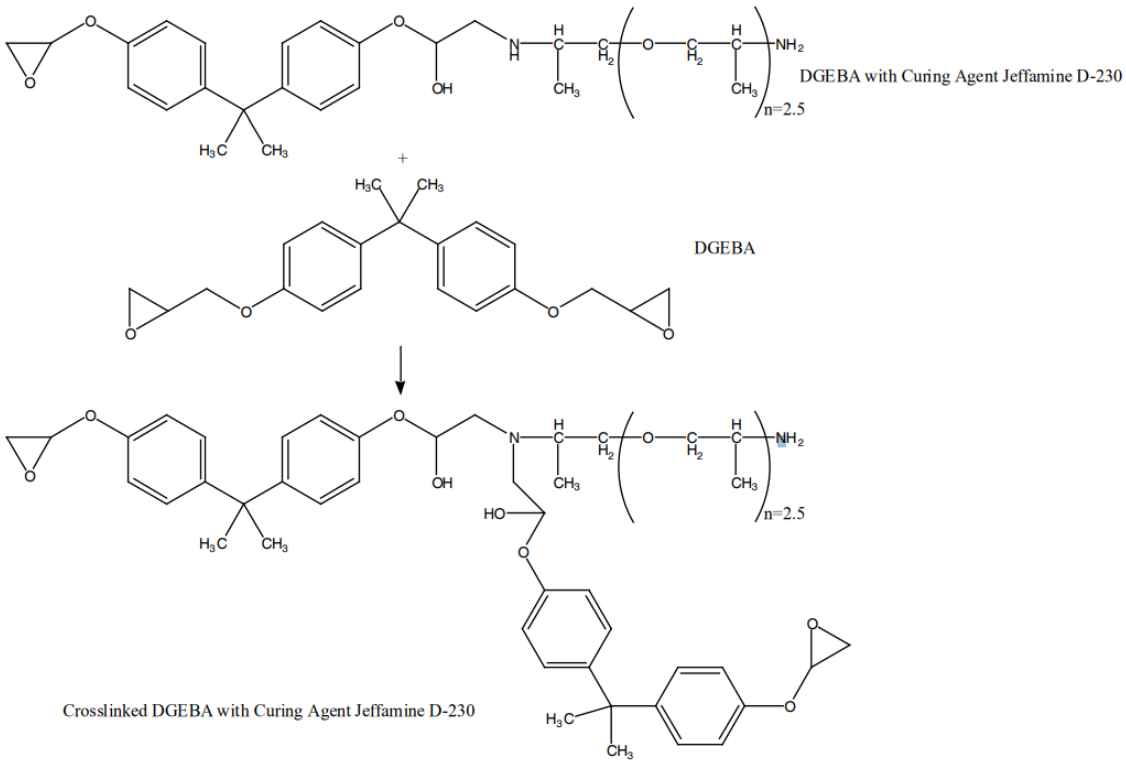

Figure 2.3: Cross-linking process to produce an epoxy polymer is started by the reaction of a DGEBA-Jeffamine D-230 hybrid with DGEBA monomer. Adapted from F. Zaragoza et al. [17].

By introducing filler materials into the epoxy resin, the thermal, mechanical and dielectric properties can be enhanced. Inorganic oxide nanoparticles are most prevalent in literature and will be in focus here. Non-oxide inorganic filler materials can be added to epoxy, but they are rarely used to enhance the dielectric properties [18]. Three different

types of inorganic oxide nanoparticles will be discussed: silicon dioxide (SiO_2, silica), titanium dioxide (TiO_2, titania) and aluminium oxide (Al_2O_3, alumina). Amorphous silica has a band grap of 8.9 eV and is therefore an electrical insulator [19]. When silica nanoparticles are used as filler in hybrid epoxy nanocomposites, the amorphous phase is most often utilized for property enhancement. The rutile and anatase phase of titania nanoparticles are the most prevalent phases in epoxy nanocomposites and have band gaps of 3.4 and 3.6 eV, respectively, [20] which also makes them electrical insulators. The most used phases of alumina are the amorphous and corundum phases which have band gaps of 6.4 and 8.8 eV respectively [21]. SiO_2 nanoparticles were used in previous project work related to this master's thesis which is why they are part of the introduction [22].

Inorganic oxide filler particles of nanometer size will have a larger surface area to interact with the surrounding polymer chains in the epoxy matrix compared to micrometer sized particles of equal weight percent of filler material. It is suspected that these interactions can induce an interfacial region between the epoxy and the inorganic particles by a behaviorial change of the organic chains surrounding the nanoparticles, which subsequently affects the properties of the nanocomposite [4]. However, nanoparticles have high surface energy which often leads to agglomeration. In addition, the compatibility between the hydrophilic inorganic oxide nanoparticles and the hydrophobic organic polymer chains is poor which further contributes to agglomeration and larger agglomerate size. A composite with well-dispersed filler particles will have a larger interaction area between the organic polymer and inorganic particles compared to an agglomerated composite, which can result in enhanced thermal, mechanical and dielectric properties. Fothergill and Nelson found that using microparticles as filler material can lead to an accumulation of a large bulk charge which results in a reduction of the electrical strength of the hybrid epoxy composite [10], [23]. Many of the negative effects of microparticles could be mitigated by substituting them with nanoparticles which was demonstrated by measuring the dieletric strength of two hybrid epoxy composites with equal filler material, but different filler size. One of the composites had filler particles of 23 nm and the other had filler particles of 1.5 μm. The hybrid epoxy composite with nanoparticles as filler exhibited higher electrical strength for every measured weight load ranging from 1 % to 40 % [10].

Researchers have proposed several different models for the interfacial region between the particles and the polymer chains. Tsagaropoulos and Eisenberg proposed a two-layer model where the regions limited mobility of the chains was caused by interactions between the particles and the polymer chains [24]. This region is covered by an inner tightly bound layer and an outer loosely bound layer. Tanaka et al. [25] proposed a multicore model where the nanoparticles had an additional layer. The tightly bound layer and the outer loosely bound layer are both included in this multicore model, but it also includes an inner bonded layer if the nanoparticles have been surface functionalized by a coupling agent. The outer layer is made up of polymer chains which react weakly with the tightly bound layer in the middle. The tightly bound layer also consists of polymer chains and it reacts strongly with the inner bounded layer which is a transition region where the polymer chains chemically bond with the coupling agent to the surface of the nanoparticle [25].

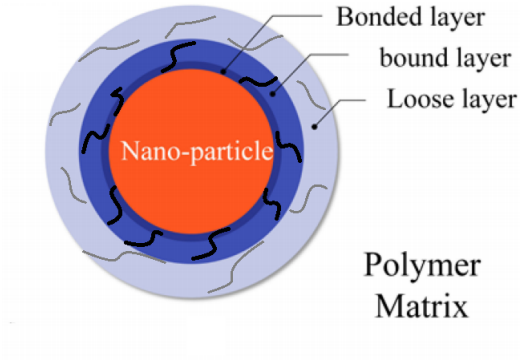

Figure 2.4: Multicore model for the interface between the polymer matrix and the nanoparticle. Adapted from T. Tanaka et al. [25]).

Surface functionalization of nanoparticles can be beneficial to prevent agglomeration. Organic molecules with a polar head group attached to long alkyl chain are frequently used to functionalize nanoparticles as they can either chemically or physically adsorb on the surface of the nanoparticle by either a coupling agent or surfactant respectively. The polar head group can help to reduce the surface energy by bonding chemically with the nanoparticle and the alkyl chain can keep the nanoparticles dispersed by steric hinderance. In addition, the hydrophobicity of the nanoparticle can increase by bonding with the polymer chains which in turn reduces the incompatibility between the inorganic particles and the organic matrix [26].

Silane coupling agents (SCAs) are often utilized to alter the surface of the inorganic oxide nanoparticles in hybrid epoxy nanocomposites [12]. These organosilicon molecules have two functional head groups where one is a functional organic group and the other is a hydrolysable group. The general empirical formula of SCAs is $R_1(CH_2)_nSi(OR_2)_3$. The OR_2 in the formula is the hydrolysable group which bonds with the surface of the particle and the R_1 is the functional group [27]. 3-aminopropyltriethoxysilane (APTES) is a very frequently used SCA for oxide nanoparticle functionalization, and will be featured in the work in this master's thesis. The structure of the APTES molecule is illustrated in figure 2.5.

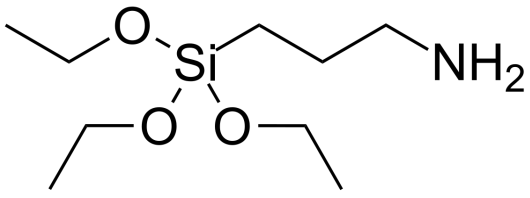

Figure 2.5: Structural visualization of APTES.

2.1.2 SiO_2, TiO_2 and Al_2O_3 epoxy nanocomposites

Several different methods have been used to find a reliable synthesis route in order to produce inorganic oxide epoxy-based nanocomposites with desireable thermal, mech-

anical and dielectric properties. Several examples of synthesis methods are mentioned in this section and they are listed in table 2.1 and 2.2. A method where the nanoparticles are nucleated and grown inside the epoxy, also known as the in situ method, is a promising method as it has the potential to achieve low degree of agglomeration and good dispersion of the nanoparticles. Two different in situ synthesis methods were tested by Metjeka et al. [28] to compare which method would potentially produce epoxy nanocomposites with the most desired properties. A one-step synthesis route was the first method where tetraethyl orthosilicate (TEOS), DGEBA, trichostatin A (TSA), H_2O and Jeffamine D2000 were mixed together simultaneously, and the second method was a two-step procedure where TEOS was hydrolyzed in a solution with TSA for 1 hr, before being mixed with Jeffamine D2000 and DGEBA. The two methods are illustrated in figure 2.6.

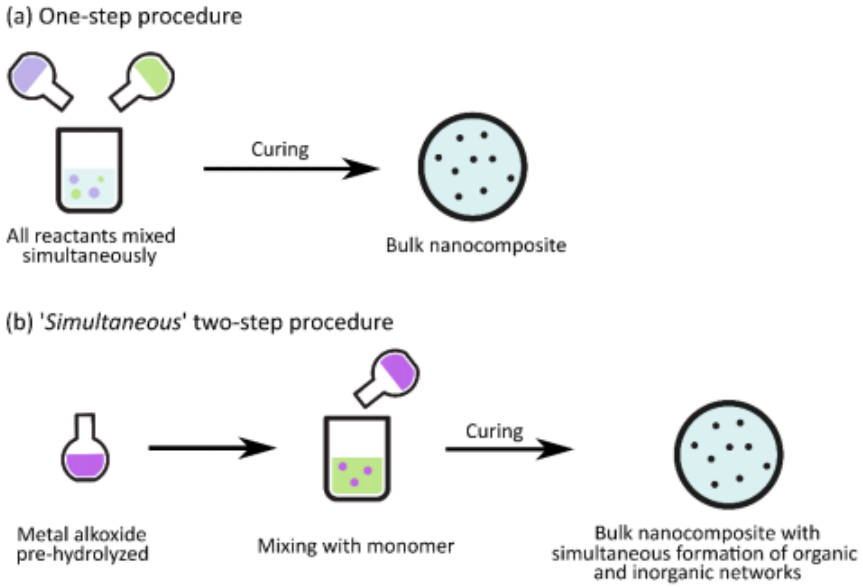

Figure 2.6: a) A one-step procedure to produce epoxy nanocomposites where all the rectants are mixed simultaneously and b) a two-step procedure where the pre-hydrolyzed metal alkoxide precursor is mixed with the epoxy monomer. Adapted from M. M. Adnan et al. [5].

The one-step procedure resulted in large SiO_2 agglomerates of approximately 100-300 nm, while the two-step method produced smaller SiO_2 agglomerates of approximately 50-100 nm. The measured dielectric loss was lower in the nanocomposites produced by both methods compared to pure epoxy, but the nanocomposites produced by the two-step method had the lowest dielectric loss.

A chronological two-step procedure was employed by Adnan et al. [5] for the synthesis of in situ SiO_2 epoxy nanocomposites where APTES and DGEBA were mixed before being added to TEOS to form a bulk nanocomposite with chemical bonds between the organic and inorganic networks in accordance with figure 2.7. The bonds between the epoxy monomer and the silane coupling agent produced nanocomposites with good dispersion of the nanoparticles and low amounts of agglomerates. The measured real

relative permittivity of the nanocomposites had approximately the same value as that of pure epoxy, but the thermal and dielectric stability of the SiO_2 epoxy nanocomposites increased compared to pure epoxy as shown by the onset of the frequency of dielectric relaxation and the glass transition temperature [5].

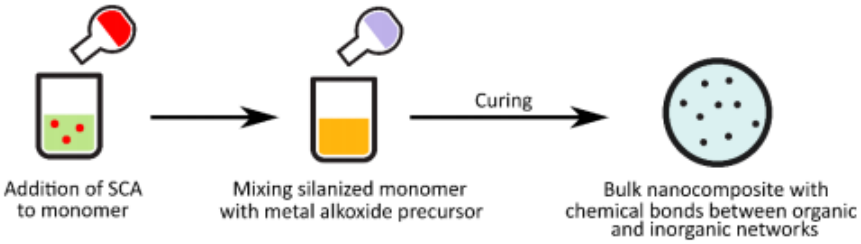

Figure 2.7: A chronological procedure to produce in situ epoxy nanocomposites where the silane coupling agent is mixed with the epoxy monomers prior to being mixed with the alkoxide precursor. Adapted from M. M. Adnan et al. [5].

Kochetov et al. presented an investigation of the dielectric properties of ex situ synthesized silica epoxy nanocomposites [29]. The SiO_2 nanoparticles were functionalized by the silane coupling agent 3-glycidoxypropyl-trymethoxysilane (GPTMS) prior to being mixed with the epoxy, and the SiO_2 filler nanoparticles were dispersed by using an ultrasonic probe followed by mechanical mixing with a Thinky mixer. An increase in the dielectric breakdown strength compared to pure epoxy was measured by performing a DC ramp test. The surface functionalization of the SiO_2 nanoparticles lead to a reorganization of the interface volume between the nanoparticles and the epoxy matrix which attributed to an increase in the dielectric breakdown strength [29].

The effects of silane coupling agents on the properties of epoxy nanocomposites was investigated by Nazir et al. [30]. SiO_2 epoxy nanocomposites with the same filler content were synthesized in situ by the chronological two-step procedure shown in figure 2.7 except for the addition of APTES for the non-functionalized samples. Transmission electron microscopy images showed distinct differences in the morphology between the epoxy nanocomposites produced with and without APTES. The SiO_2 epoxy nanocomposites without APTES had a two phase morphology where the inorganic SiO_2 was shown distinctly in the organic epoxy. This was not the case for the SiO_2 nanocomposites produced with APTES as it showed a bicontinous organic-inorganic phase morphology. Higher thermal stability and dynamic storage modulus were measured for epoxy nanocomposites produced with APTES because the silane coupling agent enhances the interphase compability which allows for better dispersion of the nanoparticles in the epoxy matrix [30].

Schadler and Nelson investigated the ex situ route to synthesize SiO_2 epoxy nanocomposites as a potential polymer for nanodielectrics in electrical insulation applications [31]. The nanoparticles were incoporated into the epoxy by mechanical shear mixing. SiO_2 epoxy nanocomposites with 2 wt% filler content were synthesized, and it was found that the dielectric breakdown strength increased by 20 % when reducing the nearest cluster distance from 75 nm to 50 nm.

Rubab et al. [32] conducted an experiment where the pre-synthesized submicron TiO_2 particles between 600 to 800 nm were used to produce epoxy composites with an ex situ method. These particles were mechanically stirred for 1 hr with the DGEBA epoxy polymer. SEM images showed that there were low amounts of agglomeration even at 5 wt% filler content. DSC measurements revealed that the glass transition temperature was higher for pure epoxy at 5 wt%, but lower at 10 wt%. The same trend was also true for the mechanical strength of the epoxy composites where the composites had the highest modulus and yield strength at 5 wt% [32].

Kurimoto et al. [33] investigated the dielectric properties of TiO_2 epoxy nanocomposites, synthesized by mixing the epoxy, curing agent and the nanofiller in that order by ultrasonification and high-pressure homogenization. Lastly, the solution was mixed again to homogenize the particle density distribution by centrifugation and larger agglomerates were attempted to be removed from the solution. Epoxy nanocomposites with smaller TiO_2 agglomerates were shown to enhance the alternating current (AC) dielectric breakdown strength (BDS) compared to composites with larger TiO_2 agglomerates and it was confirmed that the maximum agglomerate size for improving the AC BDS was 500 nm [33].

Zhang et al. [34] conducted a study of the dielectric properties of of Al_2O_3 epoxy nanocomposites. The nanocomposites were prepared by a melt mixing ex situ method. The solution was mixed for 1 hr at 60 °C by conventional mechanical stirring and ultrasonification at 20 kHz followed by another 30 min of mechanical stirring. Materials of 0, 1, and 5 wt% filler content were produced. The epoxy nanocomposite with 1 wt% Al_2O_3 generally had lower dielectric loss compared to nanocomposites with higher filler content in the frequency range from 10^{-2} to 10^6 at the same temperatures [34].

Varghese et al. [35] investigated the mechanical, thermal and dielectric properties of surface functionalized Al_2O_3 hybrid epoxy nanocomposites for high voltage insulation. The Al_2O_3 nanoparticles were functionalized with APTES or 3-Glycidoxypropyltrimethoxysilane (GPTMS) by ultrasonicating the nanoparticles in hydrogen peroxide (H_2O_2) for 12 hrs followed by mixing the nanoparticles with APTES or GPTMS in an ethanol solution which was stirred for an additional 12 hrs. Dielectric spectroscopy showed that nanocomposites with as-received Al_2O_3 nanoparticles had higher relative permittivity compared to pure epoxy whereas the functionalized composites had lower relative permittivity. However, both APTES and GPTMS functionalized nanocomposites had lower dielectric loss than pure epoxy for all frequencies. APTES functionalized Al_2O_3 epoxy nanocomposites had a 17 % and 14 % increase to tensile strength and Young's modulus respectively compared to pure epoxy, and the thermal conductivity was enhanced by 11 %. Epoxy nanocomposites treated with APTES surface functionalization had better mechanical and thermal properties compared to nanocomposites treated with GPTMS, but the dielectric properties of the epoxy nanocomposites treated with GPTMS were superior compared to APTES ones [35].

An analysis was conducted by Abdelmalik et al. [36] on TiO_2-based epoxy nanocomposites. The TiO_2 particles were anatase and had sizes ranging from 10 to 30 nm. Epoxy nanocomposites ranging from 1 to 5 wt% filler content were prepared by mixing the epoxy monomer and the curing agent in a 3:1 ratio by mechanical mixing for

3 min. This solution was placed in a vacuum oven and degassed. Lastly, the nanoparticles were incorporated into the epoxy solution by mechanical mixing. Scanning electron imaging revealed that large agglomerates up to 5 μm had formed in epoxy nanocomposites with higher filler content. Dielectric analysis showed that the relative permittivity and dielectric loss increased with increasing filler content in the TiO_2 epoxy nanocomposites [36].

Singha and Thomas [37] conducted a research project to compare the dielectric and thermal properties of hybrid epoxy composites produced with micro- and nanoparticles of TiO_2 and Al_2O_3. The TiO_2 nano-filler particles were 50 nm and the micro-filler particles were 0.5 μm while the Al_2O_3 nano- and microparticles had a size of 45 nm and 50 μm respectively. The epoxy nanocomposites were synthesized with an ex situ method by shear mechanical mixing at 700 rpm for 60 sec and ultrasonication for 1 hr. Differential scanning calorimetry showed that the glass transition temperature decreased compared to pure epoxy for epoxy nanocomposites below 5 wt% filler content. Epoxy composites synthesized with TiO_2 microparticles showed small differences in T_g compared to pure epoxy at 1 and 10 wt%. Al_2O_3-based epoxy nanocomposites generally had higher T_g than TiO_2-based epoxy nanocomposites of equal filler content. Dielectric measurements revealed that TiO_2 epoxy nanocomposites of 0.1 and 0.5 wt% filler content had lower relative permittivity and dielectric loss than pure epoxy, and the 10 wt% TiO_2 epoxy microcomposite had the highest permittivity and dielectric loss [37].

Table 2.1: Summary of selected Al_2O_3-based epoxy nanocomposite synthesis methods with the most relevant results.

Source	Dispersion method	Particle	Relevant results
[34]	Ex situ mechanical stirring and ultrasonication	Al_2O_3	Lower relative permittivity and higher dielectric loss for samples with higher filler content.
[35]	Ex situ mechanical mixing and ultrasonication	Al_2O_3	Mechanical and thermal properties superior in APTES samples compared to GPTMS. Dielectric properties superior in GPTMS samples compared to APTES, but best with non-functionalized samples.
[37]	Ex situ shear mechanical mixing and 1 hr sonication	Al_2O_3	Decreased T_g at low Al_2O_3 filler content compared to pure epoxy. Higher T_g compared to TiO_2 epoxy nanocomposites of equal filler content.

Table 2.2: Summary of selected SiO_2 and TiO_2-based epoxy nanocomposite synthesis methods with the most relevant results.

Source	Dispersion method	Particle	Relevant results
[28]	One-step and two-step in situ synthesis method.	SiO_2	Substantially larger agglomerates formed in the one-step method and the nanocomposites produced with the two-step method exhibited the lowest dielectric loss.
[14]	Chronological two-step in situ synthesis method	SiO_2	The thermal and dielectric stability of the nanocomposites increased compared to pure epoxy.
[29]	Ex situ mechanical mixing and sonication	SiO_2	Dielectric breakdown strength increased compared to pure epoxy.
[30]	Chronological two-step in situ synthesis method	SiO_2	Increased thermal stability and higher dynamic storage modulus compared to pure epoxy.
[31]	Ex situ mechanical shear mixing	SiO_2	Dielectric breakdown strength increased by 20 % by reducing the nearest cluster distance from 75 to 50 nm.
[32]	Ex situ mechanical stirring	TiO_2	Glass transition temperature and mechanical strength increased up to 5 wt% compared to pure epoxy.
[33]	Ex situ ultrasonication, centrifugation and homogenization	TiO_2	AC BDS increased for nanocomposites with smaller agglomerates and AC BDS increased for nanocomposites with agglomerates up to 500 nm.
[36]	Ex situ mechanical mixing	TiO_2	Large agglomeration formation up to 5 μm. Relative permittivity and dielectric loss increased with increasing TiO_2 filler content.
[37]	Ex situ hear mechanical mixing and 1 hr ultrasonication	TiO_2	Decreased T_g at low TiO_2 filler content compared to pure epoxy. Improved dielectric properties of 0.1 and 0.5 wt% TiO_2 nanocomposites compared to pure epoxy.

2.2 Dielectrics and dielectric properties

2.2.1 Dielectric materials

When an external electric field is applied, a dielectric prevents electrons from flowing freely through the material. The electrical energy transfer occurs via polarization of the dipoles. As a result of this effect, dielectrics are able to store electrical energy which makes them useful in capacitors [38].

When a dielectric is introduced to an external electric field, an electric displacement field is induced in the material. The electric displacement field describes how electric charges are organized in a given medium.

$$D_i = \epsilon_0 E_i + P_i \tag{2.1}$$

D_i is the dielectric displacement vector, ϵ_0 is the dielectric permittivity in vacuum, E_i is the external electric field and P_i is the polarisation [39].

The vacuum permittivity describes the ability of an electric field to permeate free space. Relative permittivity, ϵ_r is a materials absolute permittivity divided by ϵ_0. The relative permittivity is also known as the dielectric constant, κ.

2.2.2 Complex permittivity

The complex permittivity of a dielectric is the response of the material to an external electric field and the dielectric losses associated with this response. The response is often dependent on the frequency of the electric field, which indicates that the polarisation of a real material does not instantly change. The permittivity is therefore given as a complex function of the applied fields angular frequency, ω [40].

The complex permittivity consists of two parts: the real permittivity, $\epsilon^{'}$, and the imaginary permittivity, $\epsilon^{''}$ [40].

$$\epsilon(\omega) = \epsilon^{'}(\omega) - i\epsilon^{''}(\omega) \tag{2.2}$$

As the frequency of the external electric field increases, a phase difference between the directional field and the electric field emerges. This phase difference is represented by a loss angle, δ, and the tanδ describes the dielectric loss [40].

$$tan\delta = \frac{\epsilon^{''}}{\epsilon^{'}} \tag{2.3}$$

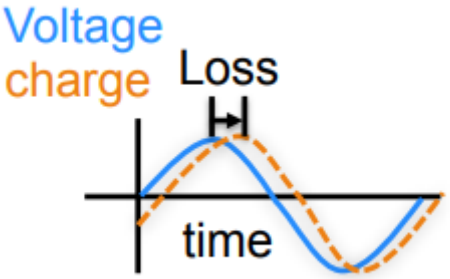

Figure 2.8: Phase difference between input and output signals in a material at constant frequency measured by impedance spectroscopy [41].

Electrically insulating materials should ideally have low dielectric loss. A high dielectric loss in a material can potentially lead to dielectric heating, which in turn can cause thermal aging and breakdown. For hybrid epoxy composites with micron sized particles, the dielectric loss of the composite increases [10], [42]. A reduction of tanδ can be achieved by replacing microparticles with nanoparticles at low filler content [37], [43] . It has been reported by Siddabattuni et al. that the dielectric loss can be further decreased by surface functionalizing the nanoparticles with organophosphate ligands [8]. Research by Yeung and Vaughan supports this as they also reported a reduction in the dielectric loss by functionalizing the nanoparticles in epoxy nanocomposites [3]. For epoxy nanocomposites, an onset of the β-relaxation was observed by Adnan et al. [14] in the 10^3 to 10^4 Hz frequency range. This type of relaxation arises due to localized rotational fluctuations of the dipoles of the O-H groups in the epoxy polymer chains which is why it is classified as a β-relaxation [44].

2.3 Thermal properties

Dielectrical properties are not the only properties to consider with respect to performance when using epoxy nanocomposites as insulators in high voltage applications. Epoxy polymer is a thermoset so both its mechanical and dielectric properties are related to the glass transition temperature, T_g. The glass transition temperature is the temperature at which the epoxy polymer transitions from a hard, glass-like state to a rubbery and viscous state, which further results in changes of the physical properties of the material [23]. A high T_g is desired for epoxy nanocomposites as it allows for elevated temperatures without breakdown.

3 Experimental

3.1 List of chemicals

Table 3.1 lists the chemicals used during the ex situ synthesis of epoxy nanocomposites. The structures of Bisphenol-A-diglycidyl ether, poly(propylene glycol) bis(2-aminopropyl ether) and the silane coupling agent were shown in figures 2.1, 2.2 and 2.5.

Table 3.1: List of the chemicals used in the ex situ hybrid epoxy nanocomposite synthesis.

Name of chemical	Abbreviation	Producer	Purity [%]
Bisphenol-A-diglycidyl ether	DGEBA	Sigma-Aldrich	< 99
Poly(propylene glycol) bis(2-aminopropyl ether)	PPGEA	Sigma-Aldrich	< 99
3-aminopropyltriethoxysilane	APTES	Sigma-Aldrich	< 99
Aluminum oxide	Al_2O_3	Sigma-Aldrich	100
Titanium(IV) oxide	TiO_2	Sigma-Aldrich	100
Ethanol	EtOH	VWR	96
Acetic acid	CH_3COOH	VWR	< 99

3.2 Surface functonalization

The functionalization of the inorganic oxide nanoparticle surface was adapted from a method developed by Hermanson [45]. Ethanol (96 vol %, 50 mL), acetic acid (99 % conc.) and APTES (99 % conc., 1 mL) were added to a beaker to a pH of 5 and the solution was stirred for 10 min with magnetic stirring at 300 rpm. Oxide inorganic nanoparticles (TiO_2 or Al_2O_3, 1 g) were added to the solution which was mixed for 24 hrs to let APTES chemically react on the nanoparticle surface. The first functionalization process was conduced with an open system (APTES#1) and the rest were conduced in a closed system (APTES#2) to reduce ethanol evaporation. The solution was centrifuged (5 min, 3000 rpm) and rinsed with ethanol three times to remove excess APTES. The final slurry was dried at 100 °C for 24 hrs.

3.3 Ex situ nanocomposite synthesis

Poly(propylene glycol) bis(2-aminopropyl ether) (PPGEA, 21.4 mL) was added to a beaker. Functionalized or as-received oxide nanoparticles were weighed in a fume hood and added to the solution in small amounts at a time to reduce agglomeration. Magnetic stirring was used to provide contineous stirring of the nanoparticles in the solution at 300 rpm. When all the nanoparticles were added, a hand mixer was used to further mix the nanoparticles in the solution and dissolve remaining visible agglomerates. Lastly, an ultrasound probe (30 % amplitude, 30 sec, 3 intervals) was used

to prevent the nanoparticles from agglomerating and break up any agglomerates that may have formed.

The curing agent solution was mixed with epoxy (DGEBA) and placed in a vacuum chamber for 5 min to remove air bubbles that may have formed during the mixing. This solution was transferred to a silicon mold. The mold produced disc-shaped samples with a diameter of 40 mm and 2 mm thickness which was further cured at 100 °C for 5 hrs. Twelve different hybrid epoxy nanocomposites were made, as listed in table 3.2. All the samples are identified based on the type of nanoparticle used and the filler content. For example, the EMHT3 sample contains TiO_2 nanoparticles with a filler content of 3 wt%. If the sample name ends with -APTES it means that the particles used to produce the nanocomposite have been functionalized with APTES.

Table 3.2: TiO_2 and Al_2O_3 epoxy nanocomposite samples synthesized with corresponding weight percentages. Surface functionalized samples have APTES in their sample name.

Sample name	Nanoparticle	Weight percent oxide [%]
Pure epoxy	-	-
EMHT1	TiO_2	1
EMHT3	TiO_2	3
EMHT5	TiO_2	5
EMHT1-APTES	TiO_2	1
EMHT3-APTES	TiO_2	3
EMHT5-APTES	TiO_2	5
EMHA1	Al_2O_3	1
EMHA3	Al_2O_3	3
EMHA5	Al_2O_3	5
EMHA1-APTES	Al_2O_3	1
EMHA3-APTES	Al_2O_3	3
EMHA5-APTES	Al_2O_3	5

3.4 Characterization

3.4.1 Fourier transform infrared spectroscopy

As-received and functionalized TiO_2 and Al_2O_3 nanoparticles were measured by Fourier transform infrared spectroscopy with the Bruker Vertex 80x spectrophotometer using the Bruker Platinum ATR diamond. A background scan was measured and 70 % ethanol was used to wipe the ATR diamond clean between each measurement. All spectra acquired had a resolution of 4 cm^{-1} using 32 scans.

3.4.2 Thermogravimetric analysis

As-received and surface functionalized TiO_2 and Al_2O_3 nanoparticles were measured by thermogravimetric analysis by the TG-Hugin analyser. All samples were weighed in a fume hood and transferred to an alumina crucible. Prior to the thermogravimetric analysis, a background was measured using the same temperature profile as the nanoparticle samples. In the first step, the samples were heated from 25 °C to 150 ° at a rate of 10 °C min^{-1}. This temperature was maintained for 30 min before it was cooled to 25 °C. In the final step, the samples were heated from 25 °C to 800 °C at a rate of 2 °C min^{-1}. Synthetic air was used as the purging gas in all measurements.

3.4.3 Impedance spectroscopy

The hybrid epoxy nanocomposites were coated by gold using a plasma gold coater. The samples were exposed to the plasma for 30 seconds on each side of the sample. A rotating disc polisher was used to remove any excessive gold coating and the gold layer on the periphery of the discs such that there is no contact between the two sides of the samples.

After the epoxy nanocomposite sample preparation was finished, the samples were mounted between two electrodes in the sample chamber. Before each measurement, the impedance spectrometer was calibrated by removing any built-up leftover charge in the sample chamber in order to minimize the uncertainty in the results and avoid artifact measurement points. The real permittivity and dielectric loss were measured as a function of frequency in a frequency range of 10^{-1} Hz to 10^{6} Hz.

3.4.4 Surface area measurements

Nitrogen adsorption was used to measure the specific surface area of the surface functionalized and non-surface functionalized inorganic oxide nanoparticles. The samples were degassed at 175 °C for 12 hrs prior to the the analysis. The specific surface area was measured with nitrogen adsorption by the 3Flex 3500 Chemisorption Analyzer at a temperatue of 83 K and the surface area was calculated using the Braunauer-Emmett-Teller (BET) technique. Nanoparticle sizes were calculated by using the BET specific surface area and the density shown in equation 3.1.

$$d_{BET} = \frac{6000}{\rho_{NPs} S_{BET}} \tag{3.1}$$

The particle size was calculated with the assumption that the particles are not porous and have a spherical shape.

3.4.5 Scanning (transmission) electron microscopy

Nanoscale imaging of various epoxy nanocomposites was performed on the SU9000 electron microscope at NTNU Nanolab cleanroom with an acceleration voltage between 10 to 30 kV. The average agglomerate size and free path length (distance between agglomerates) were manually measured after the images were captured. The samples were prepared by cutting a slice (approx. 1 mm) from bulk samples with a microtome. The slice was further cut with an ultramicrotome to 80-100 nm slices in a bath of deionized water. Finally, these nanoslices were transferred to small copper grids and dried at room temperature for 24 hrs.

3.4.6 Differential scanning calorimetry

Differential scanning calorimetry was performed on pure epoxy and the epoxy nanocomposites (approx. 5 mg) using the Netzch DSC 214 Polyma to measure the glass transition temperature. Smaller samples were cut from bulk samples by a microtome to fit in the crucibles used in the experiment. The samples were heated up from 35 to 250 °C and cooled down from 250 to 35 °C. This cycle was repeated four times, and the glass transition temperature was determined from the local maximum point of the heat capacity in the last cycle.

3.4.7 Raman Spectroscopy

Raman spectra of as-received and functionalized TiO_2 nanoparticles was recorded on a WITec Alpha 300R spectrophotometer using a monochromatic diode laser ($\lambda = 532$ nm) with a power of 20 mW. The spectra were obtained by collecting 10 accumulations with an integration time of 10 sec for each accumulation.

4 Results

The TiO_2 nanoparticles seemed more susceptible to moisture and had a higher tendency to stick together when being mixed with the curing agent compared to Al_2O_3 nanoparticles. Additionally, the Al_2O_3 nanoparticles mixed more easily with the curing agent and the curing agent dispersions with Al_2O_3 nanoparticles looked more homogeneous than the TiO_2 curing agent dispersions.

4.1 Characterization of surface functionalized nanoparticles

4.1.1 Fourier transform infrared spectroscopy

The FTIR spectra of TiO_2/TiO_2-APTES and Al_2O_3/Al_2O_3-APTES are shown in figure 4.1 and 4.2, respectively. Both FTIR spectra have the same general trend throughout the whole wavenumber range compared to their APTES counterparts. The bands at 464 cm^{-1} and 730 cm^{-1} correspond to Ti-O stretching vibration and Ti-O bending vibration, respectively, in the anatase phase of TiO_2 and the broad band ranging from 3100 to 3700 cm^{-1} corresponds to O-H stretching vibration. A band measured at 1460 cm^{-1} in the TiO_2-APTES spectra was not measured in the TiO_2 spectra. This band corresponds to a CH_2 bending vibration and this functional group can be found in APTES. The two bands at 2850 and 2920 cm^{-1} correspond to the CH_2 stretching vibration which is another characteristic band from APTES. However, this functional group can also be found in ethanol, which might explain why these bands also appear in the TiO_2 spectra as the FTIR ATR diamond has to be cleaned with ethanol before it can be used.

The bands in the IR spectra of the Al_2O_3/Al_2O_3-APTES at 510, 750 and 800 cm^{-1} correspond to Al-O stretching vibration and Al-O bending vibration, respectively. A characteristic band from APTES was measured in the Al_2O_3-APTES spectra at 1530 cm^{-1} which corresponds to a N-H bending vibration. Two other characteristic bands from APTES were measured at 2850 and 2920 cm^{-1} which correspond to the CH_2 stretching vibration. The observed bands measured for all samples with their assignment are given in table 4.2.

Table 4.1: IR bands observed for TiO_2 and TiO_2-APTES with corresponding assignments.

Wavenumber [cm^{-1}]	Functional group
464	Ti-O (stretching vibration)
730	Ti-O (bending vibration)
950	Si-O-Si (bending vibration)
1100	Si-O-Si (stretching vibration)
1460 (only TiO_2-APTES)	H-C-H (bending vibration)
2850 and 2920	H-C-H (bending vibration)
3300 (only TiO_2)	O-H (streching vibration)

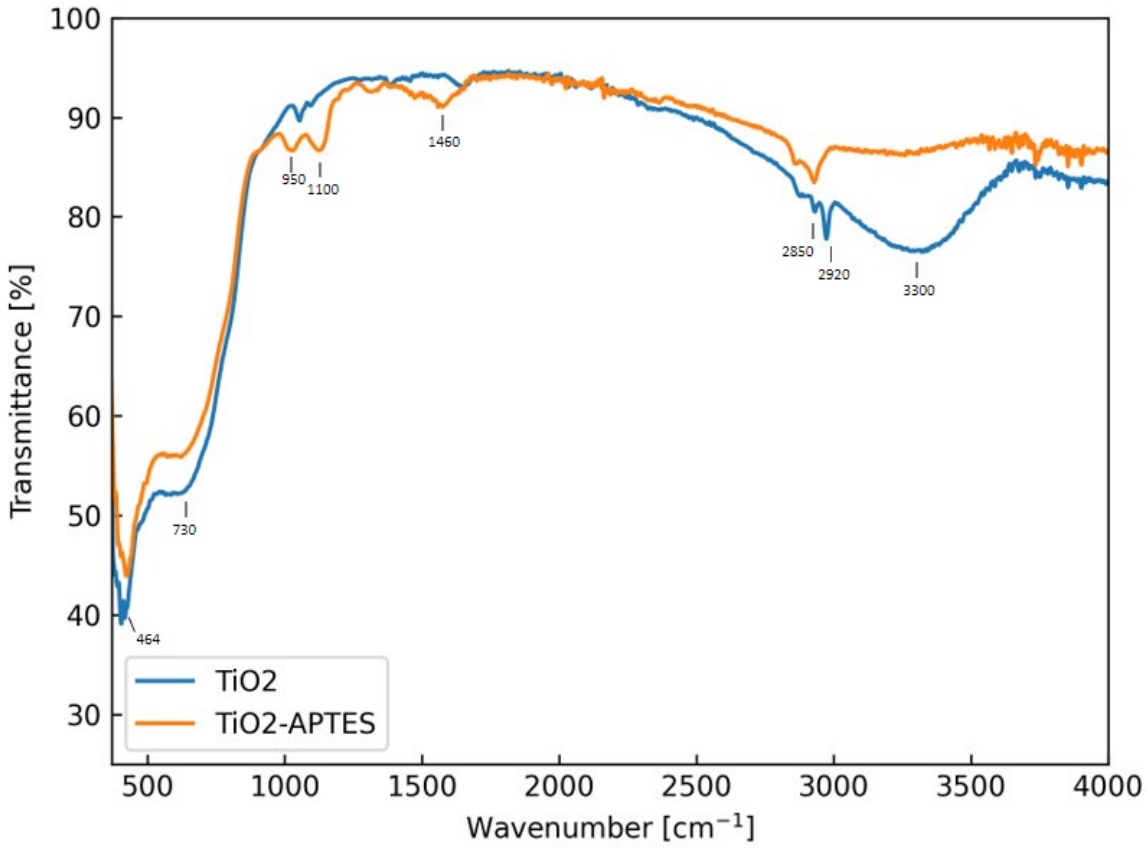

Figure 4.1: FTIR spectra of TiO_2 and TiO_2-APTES nanoparticles in the wavenumber range from 400 to 4000 cm^{-1}.

Table 4.2: IR bands observed for Al_2O_3 and Al_2O_3-APTES with corresponding assignments.

Wavenumber [cm^{-1}]	Functional group
510	Al-O (stretching vibration)
750 and 800	Al-O (bending vibration)
950	Al-OH (stretching vibration)
1530	H-C-H (bending vibration)
2850 and 2920 (only Al_2O_3-APTES)	H-C-H (stretching vibration)

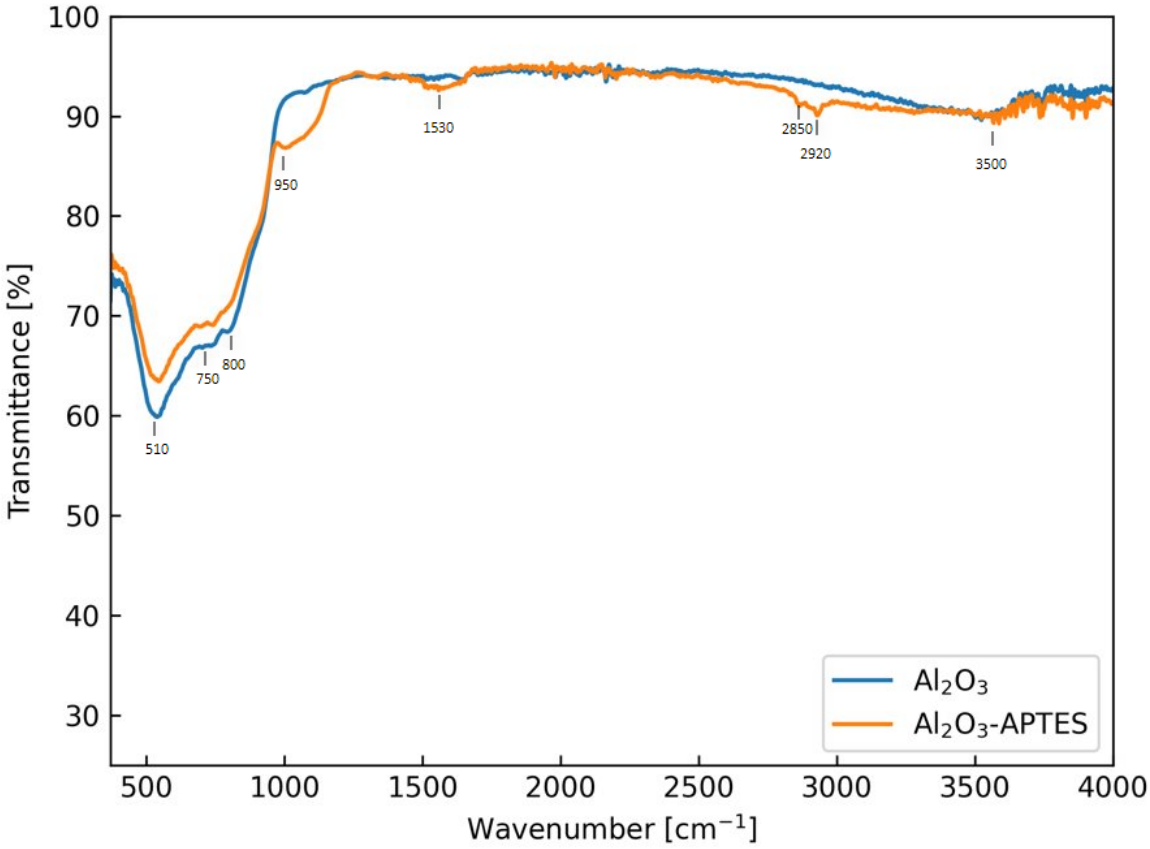

Figure 4.2: FTIR spectra of Al_2O_3 and Al_2O_3-APTES nanoparticles in the wavenumber range from 400 to 4000 cm^{-1}.

4.1.2 Raman Spectroscopy

The Raman spectra of as-received and functionalized TiO_2 nanoparticles in figure 4.3 show a narrow band at 144 cm^{-1} corresponding to the E_g mode was only observed for the crystalline anatase phase of TiO_2. The modes at 397, 519 and 638 cm^{-1} are also present in the anatase phase in addition to the rutile phase of TiO_2, but due to the relatively low intensity of these bands compared to the mode at 144 cm^{-1}, it can be assumed that the TiO_2 nanoparticles are only in the crystalline anatase phase. A band at 1100 cm^{-1} was only present in the TiO_2-APTES spectra which corresponds to the Si-O-Si vibration mode in APTES which further shows that the functionalization process of the oxide nanoparticles was successful. Table 4.3 lists the bands observed for the TiO_2 and TiO_2-APTES nanoparticles.

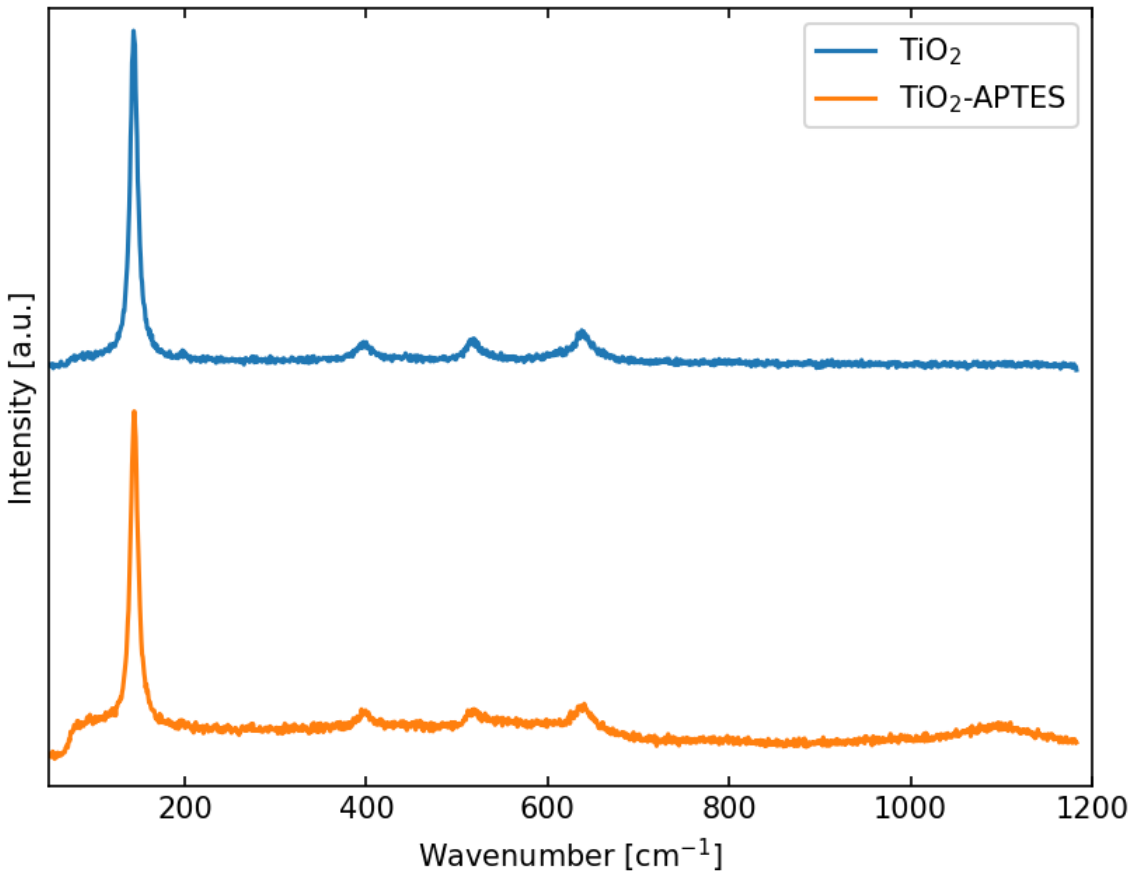

Figure 4.3: Raman spectra of TiO_2 and TiO_2-APTES nanoparticles in the wavenumber range from 0 to 1200 cm^{-1}.

Table 4.3: Raman bands observed for TiO_2 and TiO_2-APTES nanoparticles with corresponding vibration modes.

Wavenumber [cm^{-1}]	Vibration mode
144	E_g
397	B_{1g}
519	A_{1g}
638	E_g
1100 (only TiO_2-APTES)	Si-O-Si

4.1.3 Surface area measurement and thermogravimetric analysis

The surface area (S_{BET}) of as-received and functionalized TiO_2 and Al_2O_3 nanoparticles was calculated with the BET method and the particle size (d_{BET}) was calculated using S_{BET}.

Mass loss as a function of temperature for the as-received and functionalized oxide nanoparticles are shown in figure 4.4 and 4.5. The temperature range from 100 to 800 °C is chosen such that the mass loss is mostly contributed by the combustion of organic material. The TiO_2-APTES#1 and TiO_2-APTES#2 measurements represents the mass loss from functionalization of TiO_2-APTES nanoparticles in an open and closed system respectively, and the same is the case for Al_2O_3-APTES#1 and Al_2O_3-APTES#2. The mass loss of organic molecules of the TiO_2-APTES#2 was 4 wt% and the TiO_2-APTES#1 sample had a mass loss of 15 wt%. The difference in mass loss between these two samples is high, which might indicate that ethanol may have evaporated in TiO_2-APTES#1 sample. This is also the case for the Al_2O_3-APTES samples, where the Al_2O_3-APTES#2 sample had a mass loss of 7 wt% and the Al_2O_3-APTES#1 sample had a mass loss of 15 wt%. Mass loss combined with the surface area was used to calculate the surface coverage of APTES molecules on the TiO_2 and Al_2O_3 nanoparticles. This was done by first calculating the total surface area of the nanoparticles in the TGA sample. The total mol of APTES was then calculated by using the mass loss of organic material measured by the thermogravimetric analysis. Thereafter, the APTES density could be calculated by dividing the total mol of APTES by the total surface area from the BET surface area measurements. Finally, the surface coverage was calculated by dividing the APTES density with an assumed theoretical maximum APTES density [46]. A detailed calculation of the surface coverage is given in the Appendix B. The surface area, particle size, mass loss and surface coverage are presented in table 4.4.

Table 4.4: Specific surface area, particle size, mass loss and APTES surface coverage for as-received and functionalized TiO_2 and Al_2O_3 nanoparticles.

Sample	S_{BET} [m^2 g^{-1}]	d_{BET} [nm]	Mass loss [%]	Surface coverage [%]
TiO_2	43 ± 2	33.2	0	-
TiO_2-APTES1	56 ± 2	25.5	15	30.9
TiO_2-APTES2	53 ± 2	27.0	4	81.7
Al_2O_3	171 ± 2	9.7	2	-
Al_2O_3-APTES1	170 ± 2	9.8	15	43.1
Al_2O_3-APTES2	161 ± 2	10.4	7	78.0

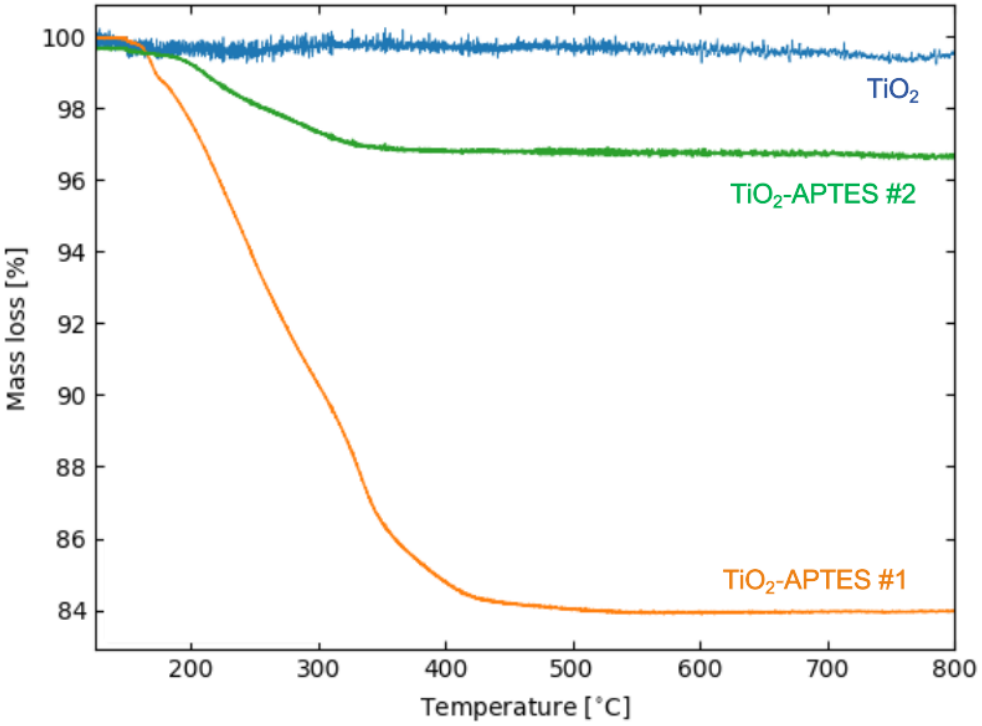

Figure 4.4: Mass loss as a function of temperature for TiO_2 and TiO_2-APTES nanoparticle samples in a temperature range from 100 to 800 °C.

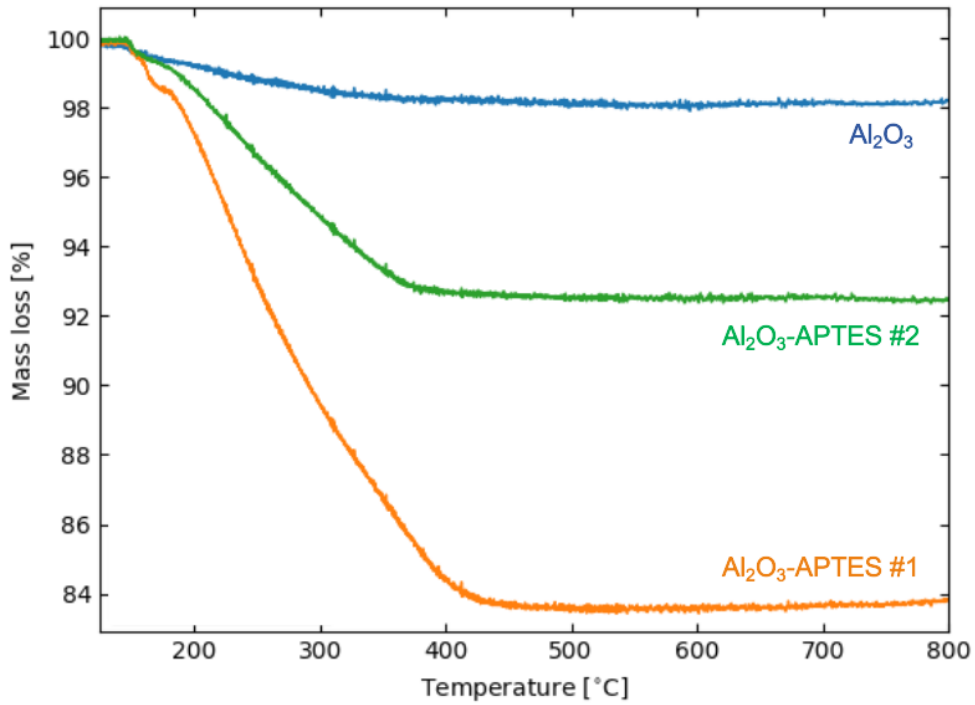

Figure 4.5: Mass loss as a function of temperature for Al_2O_3 and Al_2O_3-APTES nanoparticles sample in the temperature range from 100 to 800 °C.

4.2 Characterization of hybrid epoxy nanocomposites

4.2.1 Impedance spectroscopy

The real relative permittivity ($\epsilon^{'}$) and dielectric loss ($\tan\delta$) of pure epoxy and the twelve epoxy nanocomposites were measured by impedance spectroscopy as a function of frequency in a range of 10^{-1} to 10^{6} Hz. The samples showed the same type of dielectric relaxation at the same frequencies, but there were slight differences in both real relative permittivity and dielectric loss. The real relative permittivity are presented in figure 4.6 and 4.7, and the dielectric losses are shown in figure 4.8 and 4.9.

The dielectric relaxation between 10^{3} and 10^{6} Hz is a β-type relaxation which arise due to localized rotational fluctuations of the dipoles of the -OH groups in the epoxy chains. Pure epoxy generally has higher permittivity and lower dielectric loss compared to epoxy nanocomposites although the EMHT1 sample measured lower dielectric loss at higher frequencies and the EMHA1-APTES sample measured higher permittivity at lower frequencies. Epoxy nanocomposites with higher filler content generally show lower relative permittivity and higher dielectric loss at all frequencies compared to samples with lower filler content.

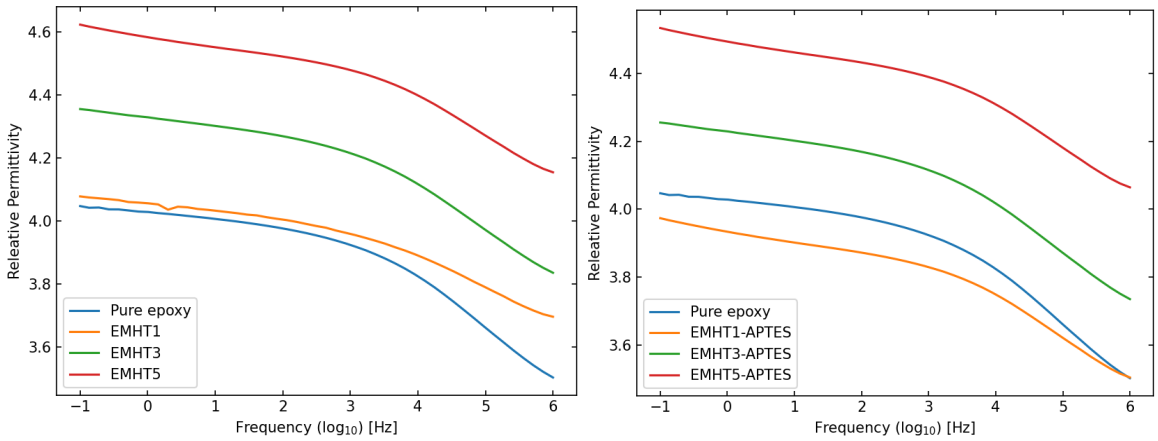

(a) (b)

Figure 4.6: Real relative permittivity of pure epoxy, (a) EMHT1, EMHT3 and EMHT5, and (b) EMHT1-APTES, EMHT3-APTES and EMHT5-APTES TiO_2-based epoxy nanocomposites as a function of frequency.

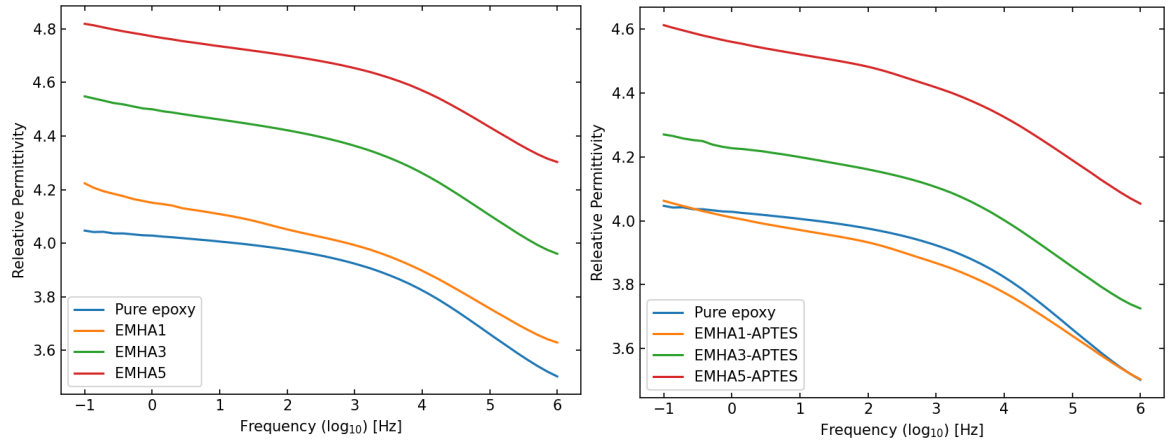

(a) (b)

Figure 4.7: Real relative permittivity of pure epoxy, (a) EMHA1, EMHA3 and EMHA5, and (b) EMHA1-APTES, EMHA3-APTES and EMHA5-APTES Al_2O_3-based epoxy nanocomposites as a function of frequency.

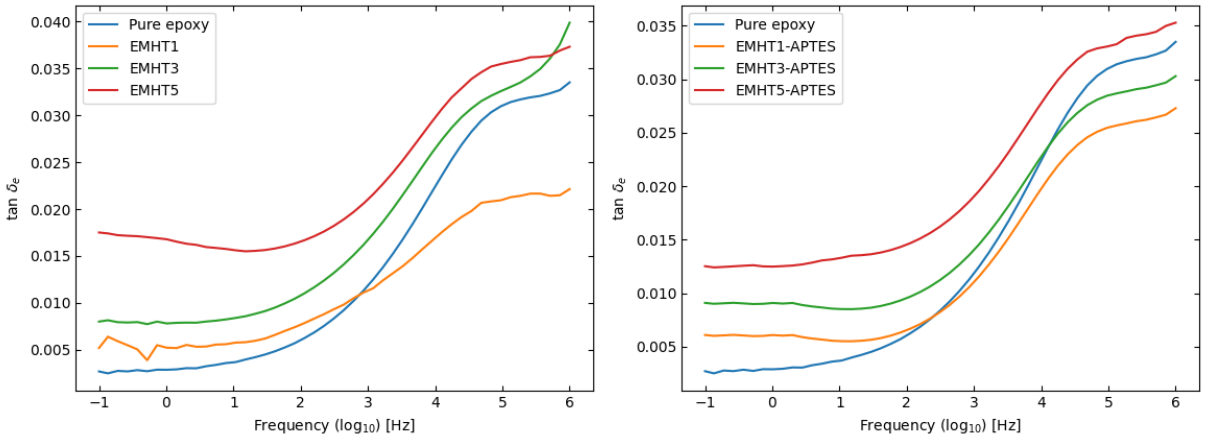

(a) (b)

Figure 4.8: Dielectric loss of pure epoxy, (a) EMHT1, EMHT3 and EMHT5, and (b) EMHT1-APTES, EMHT3-APTES and EMHT5-APTES TiO_2 epoxy nanocomposite samples as a function of frequency.

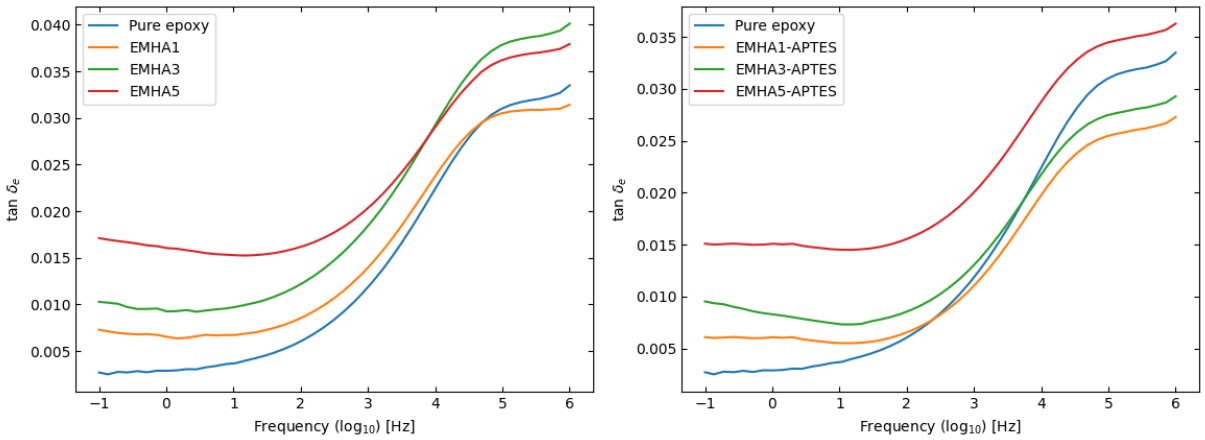

(a) (b)

Figure 4.9: Dielectric loss of pure epoxy, (a) EMHA1, EMHA3 and EMHA5, and (b) EMHA1-APTES, EMHA3-APTES and EMHA5-APTES Al_2O_3 epoxy nanocomposite samples as a function of frequency.

4.3 Nanoscale imaging

S(T)EM images were captured of a selection of the epoxy nanocomposites in order to investigate how the nanoparticles were dispersed in the epoxy matrix. The S(T)EM images shown in figure 4.10 to 4.13 were chosen as they represent the average agglomerate size and free path length of the agglomerates in the epoxy nanocomposites. TiO_2- and Al_2O_3-based nanocomposites of equal filler contents were compared to their APTES counterparts to see if the functionalization process had lead to increased dispersion and smaller agglomerates. The average agglomerate size and free path length are shown in table 4.5. Free path length was not measured for epoxy nanocomposites with 1 wt% oxide nanoparticles as it was too difficult to measure at such low filler content.

The S(T)EM images showed a broad range of agglomerates ranging from 30 nm for the smallest ones to approximately 1 μm for the largest ones. The smallest agglomerate sizes were observed in the Al_2O_3-based epoxy nanocomposite EMHA1-APTES, while the largest agglomerates were observed in the TiO_2-based epoxy nanocomposite EMHT5. Epoxy nanocomposites synthesized with Al_2O_3 nanoparticles generally had smaller agglomerates than epoxy nanocomposites synthesized with TiO_2 nanoparticles, and the Al_2O_3-based epoxy nanocomposites were more well-dispersed at higher filler content as shown in figure 4.12 and 4.13. This shows that APTES helps to prevent the nanoparticles from agglomerating to some extent and increase dispersion.

Although some of the agglomerates in epoxy nanocomposites with functionalized nanoparticles had approximately the same size as the agglomerates in epoxy nanocomposites with as-received nanoparticles, it is shown in 4.12 that the agglomerates in the epoxy nanocomposite with as-received nanoparticles are more dense compared to the agglomerates in the epoxy nanocomposite with functionalized nanoparticles. Lower

magnification S(T)EM images in figure 4.12 and 4.13 revealed that the agglomerates have relatively large free path lengths, especially high filler content and without functionalized oxide nanoparticles in the epoxy nanocomposites.

Table 4.5: Average agglomerate size and free path length of the oxide nanoparticles based on observation of the S(T)EM images.

Sample	Average agglomerate size [nm]	Average free path length [nm]
EMHT1	110	-
EMHT3	1000	800
EMHT1-APTES	35	-
EMHT3-APTES	600	700
EMHA1	100	-
EMHA3	250	300
EMHA1-APTES	30	-
EMHA3-APTES	200	200

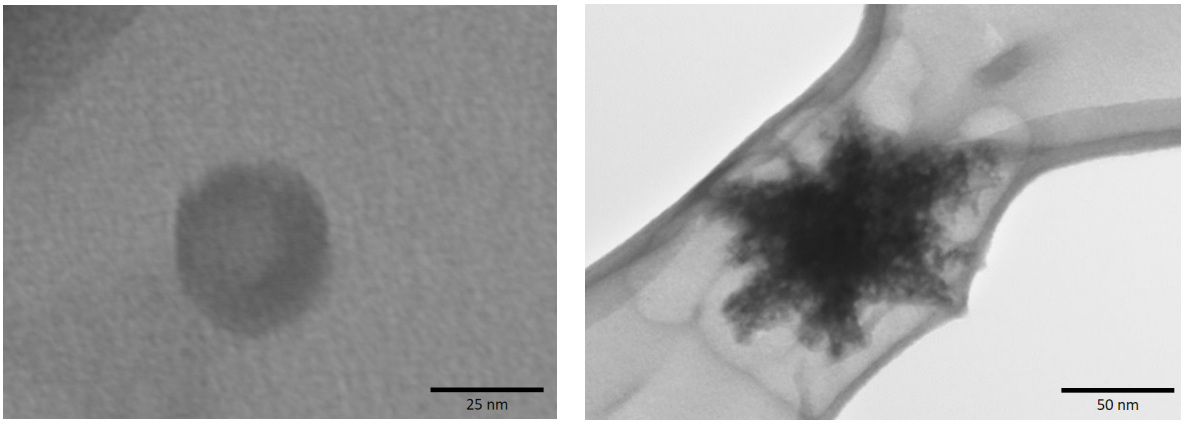

(a) (b)

Figure 4.10: S(T)EM images of (a) a small agglomerate of 30 nm observed in the functionalized Al_2O_3-based epoxy nanocomposite EMHA1-APTES and (b) a larger agglomerate of 100 nm found in the Al_2O_3-based epoxy nanocomposite EMHA1.

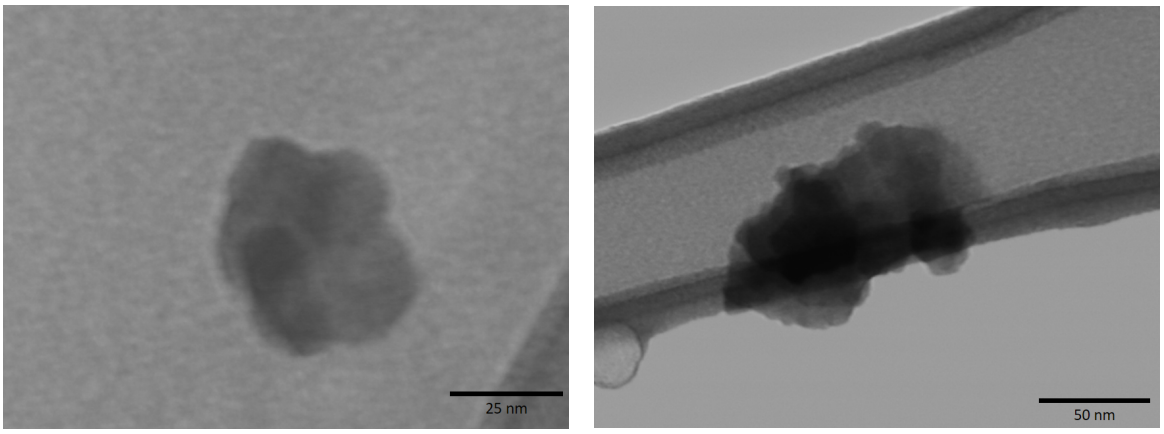

(a) (b)

Figure 4.11: S(T)EM images of (a) a small agglomerate of 27 nm observed in the functionalized TiO_2-based epoxy nanocomposite EMHT1-APTES and (b) a larger agglomerate of 100 nm found in the TiO_2-based epoxy nanocomposite EMHT1.

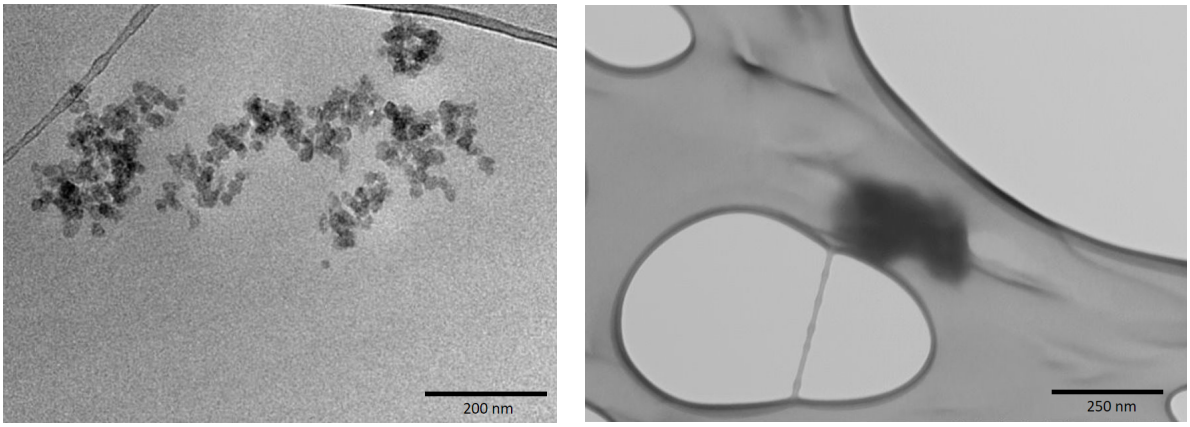

(a) (b)

Figure 4.12: S(T)EM images of (a) some larger agglomerates ranging from 50 to 300 nm found in the functionalized Al_2O_3-based epoxy nanocomposite EMHA3-APTES and (b) a large agglomerate of 300 nm found in the Al_2O_3-based epoxy nanocomposite EMHA3.

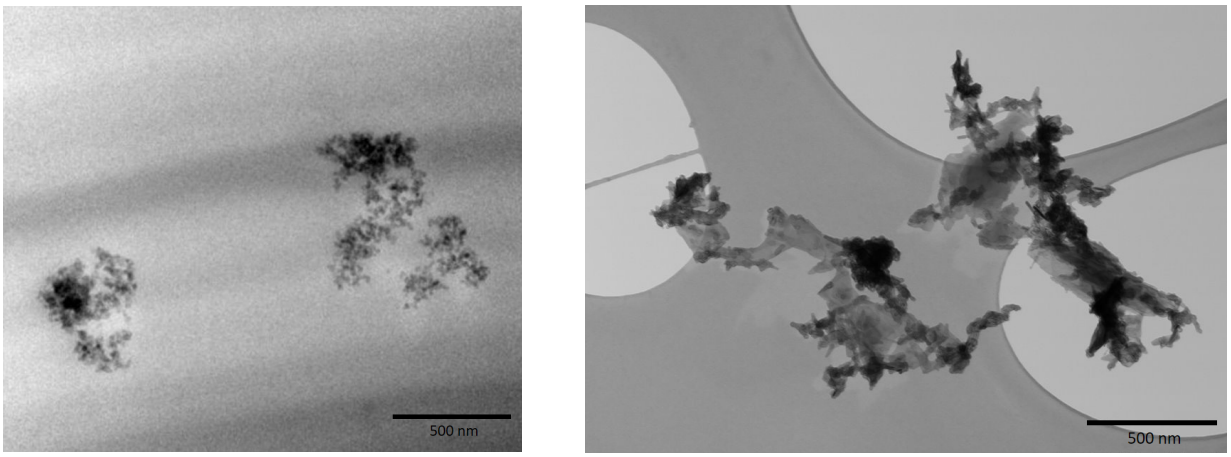

(a) (b)

Figure 4.13: Low magnification S(T)EM images of (a) some larger agglomerates ranging from 300 to 600 nm found in the functionalized TiO_2-based epoxy nanocomposite EMHT3-APTES and (b) two very large agglomerates of approximately 1 μm found in the TiO_2-based epoxy nanocomposite EMHT3.

4.4 Glass transition temperature

T_g for pure epoxy and the different epoxy nanocomposites was measured by DSC and they are shown in table 4.6. T_g was determined by the local maximum of the heat capacity in the final cycle of the DSC measurement. The addition of oxide nanoparticles at a filler content of 1 wt% initially resulted in a reduction of the glass transition temperature, but all epoxy nanocomposites were measured to have a higher glass transition temperature than pure epoxy at a filler content of 5 wt%.

Table 4.6: Glass transition temperatures, T_g, measured for pure epoxy and as-received and functionalized TiO_2 and Al_2O_3 epoxy nanocomposites.

Sample	T_g [°C]
Pure epoxy	83 ± 2
EMHT1	76 ± 2
EMHT3	82 ± 2
EMHT5	90 ± 2
EMHT1-APTES	78 ± 2
EMHT3-APTES	86 ± 2
EMHT5-APTES	93 ± 2

Sample	T_g [°C]
Pure epoxy	83 ± 2
EMHA1	76 ± 2
EMHA3	84 ± 2
EMHA5	87 ± 2
EMHA1-APTES	72 ± 2
EMHA3-APTES	78 ± 2
EMHA5-APTES	88 ± 2

TiO_2-containing samples generally showed lower T_g compared to their EMHT-APTES counterparts, but this was not the case for the Al_2O_3-based epoxy nanocomposites. A second measurement was conduced to measure the glass transition temperature of Al_2O_3 based composites which is shown in figure 4.14c.

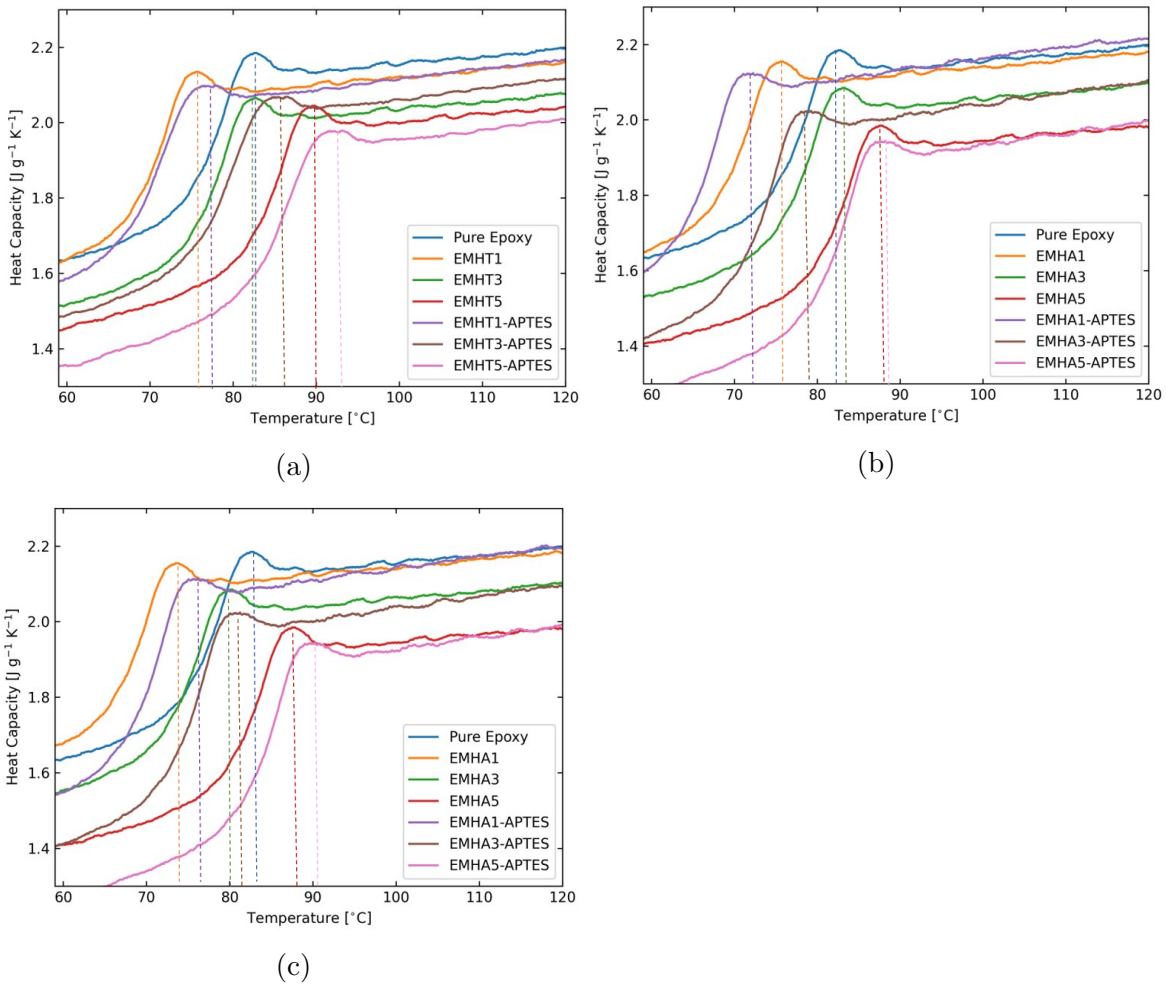

Figure 4.14: Heat capacity curves measured by DSC for pure epoxy and (a) TiO_2-based epoxy nanocomposites, (b) first measurement of the Al_2O_3-based epoxy nanocomposites and (c) second measurement of the Al_2O_3-based epoxy nanocomposites.

In the second measurement, T_g was higher for all functionalized Al_2O_3 epoxy nanocomposites compared to their non-functionalized counterparts. Furthermore, all measurements showed that T_g increased with increasing filler content, regardless of functionalization or type of oxide nanoparticle. The lowest T_g was measured for the EMHT1 and EMHA1 samples at a temperature of 76 °C and the highest T_g was measured to 93 °C for the EMHT5-APTES sample, while pure epoxy had a T_g of 83 °C.

5 Discussion

The most important results from this project are related to the the functionalized TiO_2 and Al_2O_3 nanoparticles and the dielectric and thermal properties of TiO_2 and Al_2O_3 epoxy nanocomposites. Therefore these topics will be the focus of the discussion.

5.1 Functionalization of as-received TiO_2 and Al_2O_3 nanoparticles

The FTIR and Raman spectra revealed that the oxide nanoparticles had been successfully functionalized with APTES by the observation of bands only present in APTES and not in the oxide nanoparticles. Additionally, the broad O-H band observed in the TiO_2 is not observed in the TiO_2-APTES sample which shows that the free O-H bonds at the surface of the TiO_2 nanoparticles have been replaced by APTES in a hydrolysis reaction. However, the thermogravimetric analysis and nitrogen adsorption measurements showed that the surface coverage of APTES on TiO_2 and Al_2O_3 nanoparticles were 30.9 and 43.1 % respectively. This indicates that the surface functionalization process could have been improved in order to increase the surface coverage of APTES. For example, heat could have been added to the reaction to make APTES react faster with the O-H groups on the surface of the oxide nanoparticles or the reaction time could have been increased further. Additionally, a higher vol % of APTES could have been used in the functionalization process as the current surface functionalization used a vol % of 2 % APTES and an APTES to oxide nanoparticle ratio of 1 mL APTES per 1 g oxide nanoparticles. Eduardo et al. [47] measured a large discrepancy of the surface coverage of oxide nanoparticles of different sizes which was functionalized with equal conditions. The oxide nanoparticles of 50 nm in size had an APTES density of 780 μmol/g while the 200 nm particles had an APTES density of 69 μmol/g. This shows that smaller particles have a higher silane coupling agent grafting capacity, which was expected as the effective surface area and energy is substantially higher for the smaller nanoparticles. This could explain the difference in surface coverage between the functionalized TiO_2 and Al_2O_3 nanoparticles as the TiO_2 nanoparticles had an average particle size of 33.2 nm while the Al_2O_3 nanoparticles had an average particle size of 9.7 nm.

5.2 Synthesis procedure of functionalized TiO_2 and Al_2O_3 epoxy nanocomposites

Nanoscale imaging revealed that the average agglomerate size increased drastically with increasing oxide filler wt% in the epoxy nanocomposites. The largest agglomerate size was observed in the TiO_2-based EMHT5 epoxy nanocomposite, while the smallest agglomerate size was observed in the functionalized Al_2O_3-based EMHA1-APTES epoxy nanocomposite. There are several factors which contribute to agglom-

eration formation and oxide filler content is one of them. Another factor for the difference in agglomerate size is the surface functionalization. Epoxy nanocomposites with functionalized oxide nanoparticles generally had smaller agglomerate size compared to non-functionalized epoxy nanocomposites. For example, the average agglomerate size in the EMHT1-APTES sample was 50 nm while the average agglomerate size in the EMHT1 sample was 100 nm. Additionally, the agglomerates that form in the functionalized epoxy nanocomposites are less dense than the agglomerates in the non-functionalized epoxy nanocomposites. This might be due to the steric hinderance of the long alkyl chains from APTES which is bonded to the surface of the nanoparticles. These long alkyl chains physically prevents nearby nanoparticles from agglomerating which in turn reduces the agglomerate size and improve the dispersion of the nanoparticles in the epoxy matrix. However, the agglomerate size reached up to 500 nm for the EMHT3-APTES epoxy nanocomposite.

The TiO_2-based epoxy nanocomposites generally had a larger agglomerate size compared to Al_2O_3-based epoxy nanocomposites of equal filler content. A reason for this is that the APTES surface coverage of functionalized TiO_2 nanoparticles was 30.9 % compared to 43.1 % for functionalized Al_2O_3 nanoparticles. A higher degree of APTES surface coverage leads to more pronounced steric hinderance which further reduces agglomerate size and increases particle dispersion in the epoxy nanocomposites. Additionally, the average particle size of TiO_2 was 33.2 nm compared to 10.4 nm for Al_2O_3. This means that fewer TiO_2 nanoparticles have to agglomerate in order to reach the same agglomerate size as Al_2O_3. However, smaller particles have higher surface area which means that they form agglomerates more easily to become energetically stable compared to larger particles.

The agglomerates that formed in the functionalized epoxy nanocomposites seemed to be more well dispersed compared to their as-received epoxy nanocomposite counterparts. This shows that the functionalization process of TiO_2 and Al_2O_3 has had an effect on the agglomeration formation and dispersion of the epoxy nanocomposites, which could be beneficial with respect to its dielectric properties. However, the overall dispersion of TiO_2 and Al_2O_3 nanoparticles in the epoxy nanocomposites was not ideal, and there were large distances between the nanoparticle clusters. Several different hypothetical nanoparticle dispersions was proposed by Adnan et al. [5] varying from uniform particle dispersion to large agglomerates with low dispersion, and the epoxy nanocomposites synthesized in this master's thesis resembles large agglomerates with low dispersion. The large distances between the agglomerates is a consequence of the relatively low filler contents. The as-received TiO_2 nanoparticles were observed to be very susceptible to moisture. As-received Al_2O_3 nanoparticles were also susceptible to moisture, but to a lesser extent. This could help explain the differences in agglomerate sizes in TiO_2-based and Al_2O_3-based epoxy nanocomposites, as larger agglomerates have likely formed prior to being mixed with the curing agent in the TiO_2-based epoxy nanocomposites compared to Al_2O_3-based epoxy nanocomposites and that they did not deagglomerate when being exposed to mechanical mixing and ultrasonification. More extensive use of the ultrasonic probe and more viscious stirring could improve the dispersion of the oxide nanoparticles. Uniform dispersion of hybrid oxide epoxy nanocomposites was achieved by Zheng et al. [48] by treating the epoxy mixture with an ultrasonic probe for 20 min followed by a high speed homogenizer with a rotational

speed of 24000 rpm. Although these epoxy nanocomposites were synthesized by the traditional method of mixing the oxide nanoparticles in the epoxy resin, there is good reason to believe that the dispersion and agglomeration could be improved by exposing the curing agent solution to heavier mechanical stress.

As shown in figure 4.13a and 4.13b, the agglomerates in the epoxy nanocomposite with functionalized nanoparticles are more well-dispersed compared to the epoxy nanocomposite with as-received nanoparticles. However, there is still room for improvement as the agglomerates are large compared to epoxy nanocomposites of lower filler content and the dispersion can be improved. Figure 4.13a shows three different agglomerates of inequal dispersion and size. This suggests that the dispersion could be improved by increasing the surface coverage of APTES on the surface of the TiO_2 nanoparticles. Another solution could be to use smaller nanoparticles (10-20 nm). The agglomerates in the Al_2O_3-based epoxy nanocomposites are made up of 10 nm particles compared to the 30 nm TiO_2 particles which could indicate that reducing the nanoparticle size could reduce the agglomerate size. By using smaller particles, a larger number of agglomerates might form, which might be more well-dispersed, which furthermore could improve the properties compared to the epoxy nanocomposites produced in this master's thesis.

5.3 Electrical properties

Impedance spectroscopy revealed that some of the epoxy nanocomposites with lower oxide filler content had increased dielectric properties compared to pure epoxy. As the epoxy nanocomposites in this work are synthesized for high voltage insulation applications, it is desired that they have low relative permittivity and low dielectric loss. A dielectric is polarizable, which can lead to losses when the voltage is frequency dependent. Therefore, the relative permittivity should be minimized for insulators to reduce polarizability. This will allow for the use of larger electric fields in high voltage insulation systems. In addition, the dielectric loss of an electrical insulator should be low as it could cause local dielectric heating, which in turn could cause thermal aging and lead to a breakdown [5].

The Al_2O_3-based epoxy nanocomposite EMHA1-APTES had higher relative permittivity at lower frequencies and equal relative permittivity at higher frequencies compared to pure epoxy. Additionally, the TiO_2-based epoxy nanocomposites EMHT1, EMHT1-APTES and EMHT3-APTES had lower dielectric loss than pure epoxy between the 10^3 to 10^6 frequency range. This is also the case for Al_2O_3-based epoxy nanocomposites with equal filler content and functionalization. However, most of the epoxy nanocomposites had higher relative permittivity and dielectric loss than pure epoxy. Regardless of oxide nanoparticle used and functionalization, the permittivity and the dielectric loss was increased with increasing filler content. This is likely largely due to agglomeration of the nanoparticles in the epoxy as discussed in the previous section. Abdel et al. [36] reported an increase in both the relative permittivity and dielectric loss for TiO_2-based epoxy nanocomposites with increasing TiO_2 nanoparticle filler content. However, the epoxy nanocomposite with 1 wt% TiO_2 nanoparticles had lower

dielectric loss compared to pure epoxy at frequencies above 100 Hz.

As the filler content increases, the probability of more and larger agglomerate formation increases, which in turn reduces the dielectric properties of the epoxy nanocomposite. However, surface functionalization of the oxide nanoparticles with APTES have improved the dispersion and reduced agglomerate size as shown by STEM imaging. This effect is reflected in the dielectric properties as functionalized epoxy nanocomposites generally had higher relative permittivity compared to non-functionalized nanocomposites of equal filler content. The dielectric loss was generally lower for epoxy nanocomposites with functionalized nanoparticles albeit to a lesser extent than the relative permittivity, but the EMHT1 sample had considerably lower dielectric loss than the EMHT1-APTES epoxy nanocomposite. This shows that functionalizing the oxide nanoparticles is beneficial with respect to the dielectric properties of the epoxy nanocomposites, especially at higher oxide filler content, for high voltage insulation applications. Varghese et al. [35] measured a decrease in relative permittivity and dielectric loss for epoxy nanocomposites synthesized with functionalized Al_2O_3 nanoparticles compared to epoxy nanocomposites synthesized with as-received Al_2O_3 nanoparticles of equal filler content. Additionally, the Al_2O_3-based epoxy nanocomposites had both higher relative permittivity and dielectric loss compared to pure epoxy while the epoxy nanocomposite with functionalized Al_2O_3 nanoparticles had lower relative permittivity and dielectric loss than pure epoxy.

An argument was stated by Singha and Thomas [43] that epoxy nanocomposites with small particle size, low degree of agglomeration and uniform dispersion will have the lowest permittivities and dielectric losses. This is due to the immobilization of the polymer chains, which is also dependent on the surface chemistry and the state of dispersion of the nanoparticles. If the polymer chains are immobilized, the epoxy nanocomposite will react slower to an external electric field, which in turn will reduce the relative permittivity of the epoxy nanocomposite. Additionally, Tanaka et al. [25] predicted a reduction of the polymer chain mobility with the addition of silane coupling agents as they form chemical bonds with the polymer, which in turn decreases the relative permittivity of the epoxy nanocomposite. However, the relative permittivity increased with increasing filler content in the epoxy nanocomposites. A reason for this is that the inorganic oxide filler nanoparticles have a higher relative permittivity (23-45 for anatase TiO_2 and 9 for Al_2O_3 [4]) compared to pure epoxy which will increase the permittivity of the epoxy nanocomposite as well.

When adding micrometer-sized inorganic oxide particles, the dielectric loss of the epoxy composite is generally higher compared to pure epoxy [4]. However, replacing the particles with nanoparticles, the dielectric loss is generally lower than pure epoxy at low filler content. Siddabattuni et al. [8] reported an increase of the dielectric loss of epoxy nanocomposites with 16 wt% unmodified TiO_2 nanoparticles compared to pure epoxy. The dielectric loss for epoxy nanocomposites with equal filler content, but synthesized with functionalized TiO_2 nanoparticles was also higher than pure epoxy, but lower than their unmodified counterparts. Additionally, Singha and Thomas [37] measured lower dielectric losses for epoxy nanocomposites with 1 wt% TiO_2 nanoparticles compared to pure epoxy.

5.4 Thermal properties

Nanocomposites which will be applied in high-voltage insulation should have a high T_g as it allows for elevated operational temperatures. The glass transition temperature of epoxy nanocomposites depends on many different factors such as the load and type of nanoparticle filler used, type of curing agent, epoxy nanocomposite synthesis method and whether the nanoparticles are functionalized or not. In this case, the only factors that can change T_g are the type of nanoparticle used, filler content and functionalization.

The addition of as-received and functionalized TiO_2 and Al_2O_3 nanoparticles in epoxy had noticeable effects on the glass transition temperature compared to pure epoxy as shown in table 4.6. The epoxy nanocomposites with 1 wt% filler particles had lower T_g than pure epoxy, and T_g increased with increasing filler content as shown in figure 5.1. The lowest glass transition temperature was measured for the EMHA1-APTES epoxy nanocomposite which had a T_g of 72 °C. For comparison, T_g for pure epoxy was measured to 83 °C, while the EMHT5-APTES had the highest T_g at 93 °C. The increase in T_g with increasing filler content indicates that the nanoparticles incorporate sites in the epoxy matrix which helps to prevent segmental chain motion of the epoxy nanocomposites which in turn hinders free motion of the polymer chains as the temperature increases. Functionalized epoxy nanocomposites had generally higher T_g than their non-functionalized counterparts which further suggests that the adsorption of APTES on the oxide nanoparticles prevents chain motion of the epoxy polymer when the temperature increases.

Goyat et al. [49] reported a decrease in the glass transition temperature of TiO_2-based epoxy nanocomposites at low filler content, and an increase in T_g with increasing filler content. Furthermore, Lizundia et al. [50] showed an increase in T_g of the epoxy nanocomposites when functionalizing the oxide nanoparticles, and attributed the increase in T_g to an improvement of the compatibility between the surface modified inorganic nanoparticles and the organic epoxy matrix. The energy required to overcome these interactions is increase, and thus T_g will increase. An initial decrease in T_g for lower filler content followed by increasing T_g for higher filler content in epoxy nanocomposites was reported by Adnan et al. [5]. The initial decrease in T_g was attributed to an inadequacy of local interfacial interactions, which in turn could affect the polymer chain dynamics. As the filler content of oxide nanoparticles increases, more nanoparticles chemically bond with the polymer chains, which in turn hinders free motion of the polymer chains and increases the T_g of the epoxy nanocomposite.

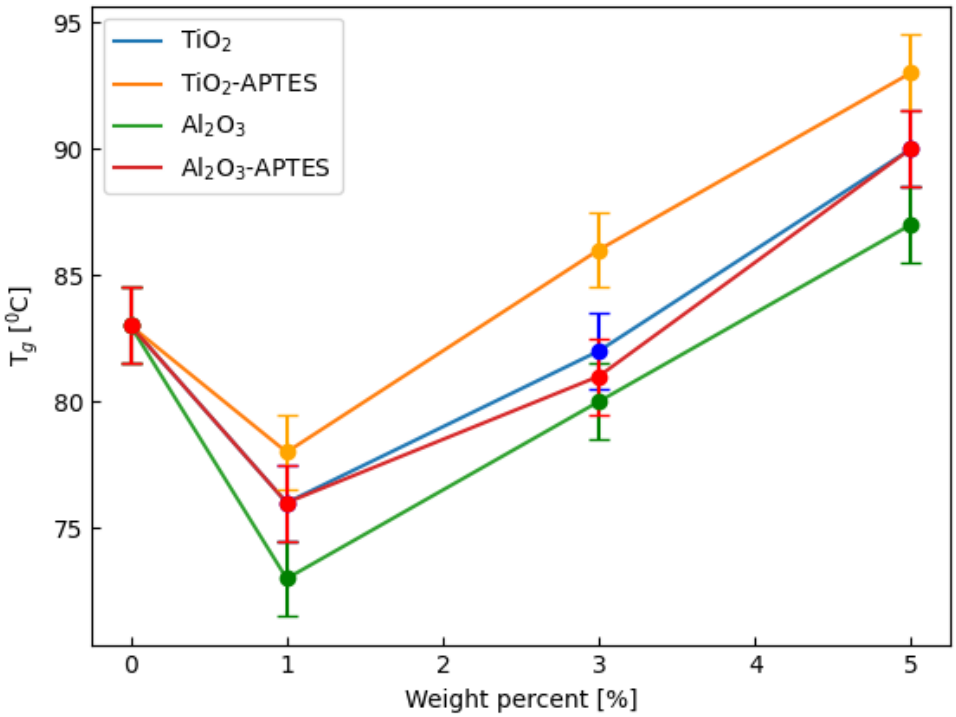

Figure 5.1: T_g as a function of wt% for pure epoxy and the TiO_2 and Al_2O_3-based epoxy nanocomposites with as-received or functionalized nanoparticles.

6 Conclusion

In this master's thesis, an investigation was carried out to see if the ex situ synthesis route of epoxy nanocomposites could be improved by mixing the inorganic filler nanoparticles with the curing agent instead of directly into the epoxy. The TiO_2 and Al_2O_3 nanoparticles were surface functionalized by APTES to reduce agglomerate size and increase the dispersion. Thermogravimetric analysis and nitrogen adsorption measurements showed that a surface coverage of APTES molecules on TiO_2 and Al_2O_3 nanoparticles of 30.9 and 43.1 %, respectively, was achieved.

Nanoscale imaging revealed that the dispersion of the TiO_2 and Al_2O_3 nanoparticles in the epoxy was low and that large agglomerates had formed, which indicates that the synthesis procedure could be improved. However, the STEM images also showed that the functionalization of the nanoparticles had a positive effect on the dispersion and agglomeration in the epoxy nanocomposites. It can therefore be concluded that the functionalization process of the nanoparticles was successful, even though it also has room for improvements.

The impedance spectroscopy revealed that the dielectric properties of the epoxy nanocomposites with high filler content had not significantly improved compared to pure epoxy. However, some of the epoxy nanocomposites with 1 wt% oxide filler content exhibited lower relative permittivity and dielectric loss than pure epoxy. Additionally, the impedance spectroscopy showed that the epoxy nanocomposites synthesized with functionalized oxide nanoparticles had lower dielectric loss and relative permittivity compared to epoxy nanocomposites of equal filler content, but with as-received oxide nanoparticles.

The glass transition temperature, T_g, for epoxy nanocomposites with 1 wt% oxide filler content was reduced compared to pure epoxy which had a T_g of 83 °C. However, the T_g increased with increasing oxide filler content and the highest T_g was measured in the TiO_2-based epoxy nanocomposite EMHT5-APTES which had a T_g of 93 °C. Additionally, TiO_2-based epoxy nanocomposites generally exhibited higher T_g compared to Al_2O_3-based epoxy nanocomposites of equal filler content and epoxy nanocomposites produced with surface functionalized oxide nanoparticles generally had higher T_g compared to as-received ones. The increase in T_g for functionalized samples could be due to the APTES adsorbed on the oxide nanoparticle surface having a reducing effect of the free motion of the polymer chains in the epoxy when the nanocomposite is being heated.

To conclude, some of the epoxy nanocomposites synthesized in this work exhibited desirable dielectric properties, especially at lower filler content of TiO_2 and Al_2O_3. However, the dielectric properties of the epoxy nanocomposites has great potential to be improved further by changing a few simple steps in the synthesis method such as increasing the ultrasonication time or adding small amounts of heat to the APTES functionalization reaction. Furthermore, this work presents a simple way to synthesize epoxy nanocomposites which can be done by using common laboratory equipment.

7 Further work

The ex situ synthesis method of hybrid epoxy nanocomposites by mixing the nanoparticles with the curing agent could be improved by:

- The use more extensive mechanical stirring or ultrasonication and see if the agglomeration rate can be decreased and the dispersion can be increased.
- APTES can be replaced with 3-glycidoxypropyltrimethoxysilane (GPTMS) in the functionalization process which could have an effect on the dielectric properties of the hybrid epoxy nanocomposites.
- The functionalization process can be modified in order to achieve a higher amount of SCA nanoparticle surface coverage.
- Small angle X-ray scattering can be utilized to measure the shape and structure of the nanoparticles in the epoxy nanocomposites.
- Tensile measurements can be performed to measure the mechanical strength of the epoxy nanocomposites and compare the results with pure epoxy.

References

[1] S. Kasap, *Principles of electronic materials and devices*. New York, United States, McGraw-Hill, 3rd edition, 2006.

[2] E. A. Campo, *Selection of Polymeric Materials: How to Select Design Properties from Different Standards (Plastics Design Library)*. New York, United States, William Andrew Publishing, 1st edition, 2008.

[3] C. Yeung and A. Vaughan, 'On the effect of nanoparticle surface chemistry on the electrical characteristics of epoxy-based nanocomposites', *Polymers*, 8: 124–128, 2016.

[4] M. M. Adnan, E. G. Tveten, J. Glaum, M. G. Ese, S. Hvidsten, W. Glomm and M. A. Einarsrud, 'Epoxy-based nanocomposites for high-voltage insulation: A review', *Adv. Electron. Mater*, 5: 1800505, 2018.

[5] M. M. Adnan, A. R. Dalod, M. H. Balci, J. Glaum and M. A. Einarsrud, 'In situ synthesis of hybrid inorganic–polymer nanocomposites', *Polymers*, 10: 1129, 2018.

[6] A. M. Rahnamol and J. Gopalakrishnan, 'Improved dielectric and dynamic mechanical properties of epoxy/polyaniline nanorod/in situ reduced graphene oxide hybrid nanocomposites', *Polymer Composites*, 41: 2998–3013, 2020.

[7] Z. Han and R. Garret, 'Overview of polymer nanocomposites as dielectrics and electrical insulation materials for large high voltage rotating machienes', *Nanotechnology*, 2: 727–732, 2008.

[8] S. Siddabattuni, T. P. Schuman and F. Dogan, 'Dielectric properties of polymer-particle nanocomposites influenced by electronic nature of filler surfaces', *ACS Appl Mater Interfaces*, 6: 1917–1927, 2013.

[9] D. Pinto, L. Bernardo, A. Amaro and S. Lopes, 'Mechanical properties of epoxy nanocomposites using titanium dioxide as reinforcement – a review.', *Construction Building Materials*, 95: 506–524, 2015.

[10] J. K. Nelson and J. C. Fothergill, 'Internal charge behaviour of nanocomposites', *Nanotechnology*, 15: 586–595, 2004.

[11] C. Rao, P. J. Thomas and G. Kulkarni, *Nanocrystals: Synthesis, Properties and Applications*. Berlin, Germany, Springer-Verlag, 1st edition, 2007.

[12] K. Sarita, K. Susheel, A. Celli, J. Njuguna, Y. Habibi and R. Kumar, 'Surface modification of inorganic nanoparticles for development of organic–inorganic nanocomposites—a review', *Progess in Polymer Science*, 38: 1232–1261, 2013.

[13] M. J. Owen, *Silicone Surface Science*. Midland, United States, Springer-Verlag, 4th edition, 2012.

[14] M. M. Adnan, E. G. Tveten, J. Glaum, M. H. Ese, S. Hvidsten, W. Glomm and M. A. Einarsrud, 'In situ synthesis of epoxy nanocomposites with hierarchical surface-modified SiO_2 clusters', *Journal of Sol-Gel Science and Technology*, 95: 783–794, 2020.

[15] L. S. Schadler, *Nanocomposite Science and Technology*. Weinheim, Germany, John Wiley Sons, Ltd, 1st edition, 2004.

[16] Q. Guo, *Thermosets*. Cambridge, United States, Elsevier Ltd, 2nd edition, 2012.

[17] F. T. Zaragoza, 'Polymer bisphenol-a, the incorporation of silica nanospheres into epoxy–amine materials and polymer nanocomposites', *Nereis. Revista Iberoamericana Interdisciplinar de Métodos, Modelización y Simulación*, 3: 17–23, 2010.

[18] T. Heid, M. Fréchette and E. David, 'Functional epoxy composites for high voltage insulation involving c-bn and reactive poss as compatibilizer', *Journal of Materials Science*, 50: 5494–5503, 2015.

[19] G. D. Wilk, R. M. Wallace and J. M. Anthony, 'High- gate dielectrics: Current status and materials properties considerations', *Journal of Applied Physics*, 89: 5243–5275, 2001.

[20] M. Dou and C. Persson, 'Comparative study of rutile and anatase SnO_2 and TiO_2: Band-edge structures, dielectric functions, and polaron effects', *Journal of Applied Physics*, 113: 083703, 2013.

[21] D. Liu, S. J. Clark and J. Robertson, 'Oxygen vacancy levels and electron transport in Al_2O_3', *Applied Physics Letters*, 96: 032905, 2010.

[22] A. S. Lien, M. M. Adnan, J. Glaum and M. A. Einarsrud, 'Hybrid epoxy nanocomposites for high voltage application', *Unpublished*, 2020.

[23] W. Weihong, L. Jingjing, W. Zheng and Q. Hongqiang, 'Preparation, curing, and properties of boron-containing bisphenol-s formaldehyde resin/o-cresol formaldehyde epoxy resin/nano-SiO_2 composites.', *Macromol. Res*, 24: 209–217, 2016.

[24] G. Tsagaropoulos and A. Eisenberg, 'Dynamic mechanical study of the factors affecting the two glass transition behavior of filled polymers. similarities and differences with random ionomers', *Macromolecules*, 28: 5981–6382, 1995.

[25] T. Tanaka, M. Kozako, N. Fuse and Y. Ohki, 'Proposal of a multi-core model for polymer nanocomposite dielectrics', *IEEE Transactions on Dielectrics and Electrical Insulation*, 12: 669–681, 2005.

[26] Y. Li, Z. Chen, X. Li and H. Zeng, 'A new surface modification method to improve the dispersity of nano-silica in organic solvents', *J Sol-Gel Sci Technol*, 58: 290–295, 2011.

[27] S. Mallakpour and M. Madani, 'A review of current coupling agents for modification of metal oxide nanoparticles', *Progress in Organic Coatings*, 86: 194–207, 2015.

[28] L. Matějka, J. Pleštil and K. Dušek, 'Structure evolution in epoxy–silica hybrids: Sol–gel process', *Journal of Non-Crystalline Solids*, 226: 114–121, 1998.

[29] R. Kochetov, I. Tsekmes, L. Chmura, P. Morshuis, T. Iizuka, K. Tatsumi and T. Tanaka, 'The effect of nanosilica on the dc breakdown strength of epoxy based nanocomposites', in *2014 IEEE Conference on Electrical Insulation and Dielectric Phenomena (CEIDP)*, 2014, 715–718.

[30] T. Nazir, A. Afzal, H. M. Siddiqi, Z. Ahmad and M. Dumon, 'Thermally and mechanically superior hybrid epoxy–silica polymer films via sol–gel method', *Progress in Organic Coatings*, 69: 100–106, 2010.

[31] L. S. Schadler and J. K. Nelson, 'Polymer nanodielectrics—short history and future perspective', *Journal of Applied Physics*, 128: 120902, 2020.

[32] Z. Rubab, A. Afzal, H. Siddiqi and S. Saeed, 'Preparation, characterization, and enhanced thermal and mechanical properties of epoxy-titania composites', *The Scientific World Journal*, 2014: 515739, 2014.

[33] M. Kurimoto, T. Umemoto, S. Yoshida, T. Mabuchi and H. Muto, 'Breakdown strength of TiO_2 epoxy nanocomposites using centrifugation agglomerate removal', *IEEE Transactions on Dielectrics and Electrical Insulation*, 28: 74–81, 2021.

[34] C. Zhang, R. Mason and G. Stevens, 'Dielectric properties of alumina-polymer nanocomposites', in *Annual Report Conference on Electrical Insulation and Dielectric Phenomena (CEIDP)*, 2005, 721–724.

[35] J. P. Varghese, A. M. Chandran, P. K. S. Mural, R. Sunitha and P. Preetha, 'Investigating the characteristics of amino silane functionalized alumina nanoparticles doped epoxy nanocomposite for high-voltage insulation', *IEEE Transactions on Nanotechnology*, 21: 227–235, 2022.

[36] A. A. Abdelmalik, M. O. Ogbobo and G. E. Momoh, 'Investigating the mechanical and insulation performance of waste eggshell powder/epoxy polymer for power insulation application', *SN Applied Sciences*, 1: 2019.

[37] S. Singha and M. J. Thomas, 'Dielectric properties of epoxy nanocomposites', *IEEE Transactions on Dielectrics and Electrical Insulation*, 15: 12–23, 2008.

[38] D. Damjanovic, 'Ferroelectric, dielectric and piezoelectric properties of ferroelectric thin films and ceramics', *Reports on Progress in Physics*, 61: 1267–1324, 1998.

[39] R. J. Tilley and R. Tilley, *Understanding solids: the science of materials.* Cardiff, Wales, John Wiley Sons Inc, 2nd edition, 2004.

[40] P. Skocik and P. Neumann, 'Measurement of complex permittivity in free space', *Procedia Engineering*, 100: 100–104, 2015.

[41] H. Mahdavi and F. Sohbatzadeh, 'The effects of applying different bias voltages and phase differences on performance of an asymmetric surface dielectric barrier discharge; an experimental investigation.', *J. Theor. Appl. Phys.*, 13: 165–177, 2019.

[42] S. Singha and M. J. Thomas, 'Dielectric properties of epoxy nanocomposites', *IEEE Transactions on Dielectrics and Electrical Insulation*, 15: 12–23, 2008.

[43] C. Zou, J. C. Fothergill and S. W. Rowe, 'The effect of water absorption on the dielectric properties of epoxy nanocomposites', *IEEE Transactions on Dielectrics and Electrical Insulation*, 15: 106–117, 2008.

[44] J. M. Pochan, R. J. Gruber and D. F. Pochan, 'Dielectric relaxation phenomena in a series of polyhydroxyether copolymers of bisphenol-a—endcapped polyethylene glycol with epichlorohydrin', *Journal of Polymer Science: Polymer Physics Edition*, 19: 143–149, 1981.

[45] G. T. Hermanson, *Bioconjugate Techniques.* Illinois, United States, Academic Press, 2nd edition, 2008.

[46] B. Qiao, T. J. Wang, H. Gao and Y. Jin, 'High density silanization of nano-silica particles using 3-aminopropyltriethoxysilane (APTES)', *Applied Surface Science*, 351: 646–654, 2015.

[47] E. J. Cuento, A. Castro, F. Suárez, S. Gálvez, V. Carmen, P. Valles and E. Mateo, 'APTES-based silica nanoparticles as a potential modifier for the selective sequestration of CO_2 gas molecules', *Nanomaterials*, 11: 2893, 2021.

[48] Y. Zheng, Y. Zheng and R. Ning, 'Effects of nanoparticles SiO_2 on the performance of nanocomposites', *Material Letters*, 57: 2940–2944, 2003.

[49] M. Goyat, S. Rana, S. Halder and P. Ghosh, 'Facile fabrication of epoxy-TiO_2 nanocomposites: A critical analysis of TiO_2 impact on mechanical properties and toughening mechanisms', *Ultrasonics Sonochemistry*, 40: 861–873, 2018.

[50] E. Lizundia, I. Serna, E. Axpe and J. L. Vilas, 'Free-volume effects on the thermomechanical performance of epoxy–SiO_2 nanocomposites', *Journal of Applied Polymer Science*, 134: 45216, 2017.

Appendix A - Risk assessment

RISK ASSESSMENT (RiskManager alternative)

Unit/Institute:	IMA	**Date:**	21.01.2022
Responsible line manager (name):	Einar Hjorthol	**Revised:**	
Responsible for activities being risk assessed (name):	Eva Rise		
Participants in the risk assement (names):	Alexander Svalheim Lien, Mari-Ann Einarsrud, Eva Rise, Mohammed Mostafa Adnan.		

Description of the activity, process, area, etc.:

In this activity, different oxide nanoparticles (TiO2 and Al2O3) will be heat treated and functionalized by a silane coupling agent (APTES). These functionalized oxide NPs will then be incorporated into a curing agent (Poly(propylene glycol) bis(2-aminopropyl ether)) by either ultrasound or mechanical methods or a combination. The curing agent will thereby be mixed with an epoxy monomer (Bisfenol-A-Diglycidyleter) to form the desired nanocomposite. Different samples will be made with oxide NP content varying from 1 to 5 wt%. These samples will be characterized with different methods including FTIR, dielectric spectroscopy, Raman spectroscopy, BET, TGA, S(T)EM and DSC.

Activity / process	**Unwanted incident**	**Existing risk reducing measures**	**Probability (P)**	**Consequence (C)** Evaluate the categories individualley. *Health should always be evaluated.*				**Risk value (P x C)**	**Risk reducing measures - suggestions**	**Residual risk after measures being implemented**
			(1-5)	Health (1-5)	Material values (1-5)	Environment (1-5)	Reputation (1-5)		Measures reducing the probability of the unwanted incident happening should be prioritized.	
Handling of Bisfenol-A-Diglycidyleter (Epoxy monomer)	Spill of chemical on skin or eyes.	Wear safety goggles, latex gloves, lab coat, long pants and lab shoes to reduce the area of exposure.	2	2				4		
Handling of 3-Aminopropyltrietoksysilan (Silane coupling agent/hardener)	Spill of chemical on skin or eyes and inhalation of chemical.	Use a fume hood when using the chemical and a closed container when transporting the chemical. Wear safety goggles, nitrile gloves, lab coat, long pants and lab shoes to reduce the area of exposure.	2	3				6	Be extra careful when using and handling this chemical due to the health hazard this chemical may provide. This can reduce the probability of health hazard.	3
Handling of Poly(propylene glycol) bis(2-aminopropyl ether) (Curing agent)	Spill of chemical on skin or eyes.	Wear safety goggles, latex gloves, lab coat, long pants and lab shoes to reduce the area of exposure.	2	3				6	Wearing a face shield instead of/in addition to regular safety goggles may reduce the risk of eye contact with the chemical.	3
Handling of (3-Glycidyloxypropyl)trimethoxysilane (Silane coupling agent)	Spill of chemical on skin or eyes.	Wear safety goggles, latex gloves, lab coat, long pants and lab shoes to reduce the area of exposure.	2	3				6	Wearing a face shield instead of/in addition to regular safety goggles may reduce the risk of eye contact with the chemical.	3
Handling of Silicon dioxide nanopar	Inhalation of Silicon dioxide powder.	Use a fume hood when using the chemical and a closed container when transporting the chemical.	2	3				6		
Heat treatment of Silcon dioxide nanoparticles	Exposure to chemical and/or unwanted reaction.	Use safety goggles, lab coat, lab shoes, long pants and fire/high temperature protective gloves when taking the chemical in and out of the oven. Make sure the oven is clean as contaminants may cause a fire or unwanted reaction or possibly an explosion when heated to a high temperature. Use a closed container.	1	3				3		
Mixing of Silicon dioxide nanoparticles and 3-Aminopropyltrietoksysilan and ethanol	Ethanol is flammable. Skin burns and material damage. The functionalization might be done using an autoclave (high pressure).	Keep the solution away from heat. Wear safety goggles, lab coat, lab shoes, long pants and nitrile gloves when handling the solution. Use a fume hood. Recieve training on how to use an autoclave properly.	2	2				4		
Ultrasonication of functionalized Silicon dioxide nanoparticles and Poly(propylene glycol) bis(2-aminopropyl ether)	Exposure to ultrasonic waves and damage to instrument,	Wear safety goggles, nitrile gloves, lab coat, long pants and lab shoes. Don't use the ultrasound for too long at a time as heat might build up.	2	2				4		

Appendix B - Calculations

Example calculation of Al_2O_3-APTES surface coverage

The total surface area of the Al_2O_3-APTES molecules from the TGA is:

$$S_{Al_2O_3} = S_{BET} \cdot m_{Al_2O_3} = S_{BET} \cdot (m_{tot} - m_{H_2O} - m_{loss}) = 171 m^2/g \cdot (10 - 2 - 0.7) mg = 1.249 m^2 \tag{B.1}$$

The number of moles of APTES released is calculated by:

$$n_{APTES} = \frac{m_{loss}}{M_{m,NH}} = \frac{0.07 \cdot 10.0 mg}{58 g/mol} = 1.206 \cdot 10^{-5} mol \tag{B.2}$$

This is calculated assuming $NH_2CH_2CH_2CH_2$-group release by combustion.

The APTES density is given by:

$$n_A^s = \frac{n_A \cdot N_A}{S_{Al_2O_3}} = \frac{1.206 \cdot 10^{-5} mol \cdot 6.022 \cdot 10^{23} molecules/mol}{1.249 \cdot 10^{18} nm^2} = 5.81 APTES/nm^2 \tag{B.3}$$

The percentage of surface covered by APTES, C [%], is then calculated as [46]:

$$C[\%] = \frac{n_A^s}{n_{A,theoretical}^s} = \frac{5.81 APTES/nm^2}{13.48 APTES/nm^2} = 43.1\% \tag{B.4}$$

Appendix C - S(T)EM images

Figure C.1 and C.2 show some additional S(T)EM images of agglomerates that formed in the different epoxy nanocomposites and the dispersion of the agglomerates. Energy dispersive X-ray spectroscopy (EDS) images of the EMHA1-APTES and EMHT1-APTES epoxy nanocomposites are shown in figure C.3.

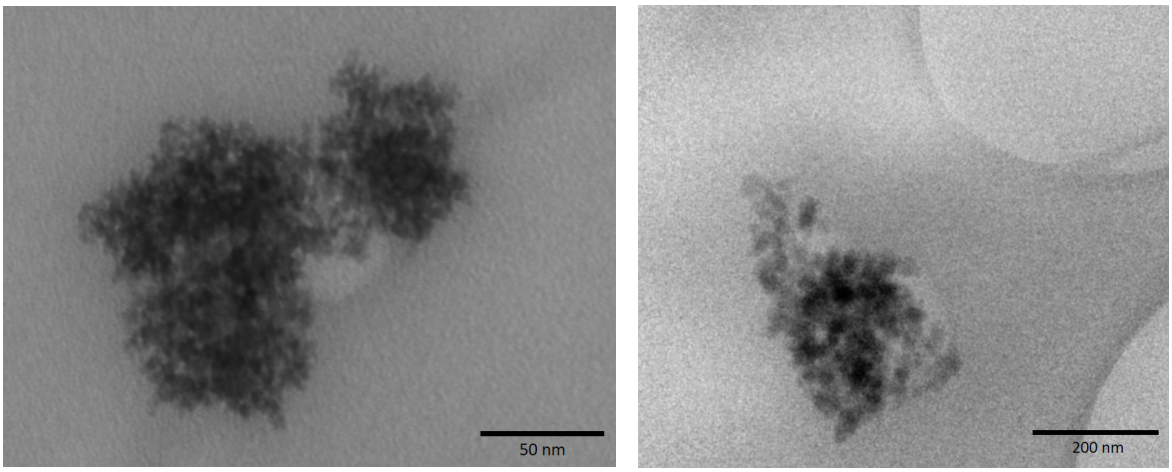

(a) (b)

Figure C.1: S(T)EM image of an agglomerate formed in the (a) EMHA1 epoxy nanocomposite, and (b) EMHT3 epoxy nanocomposite.

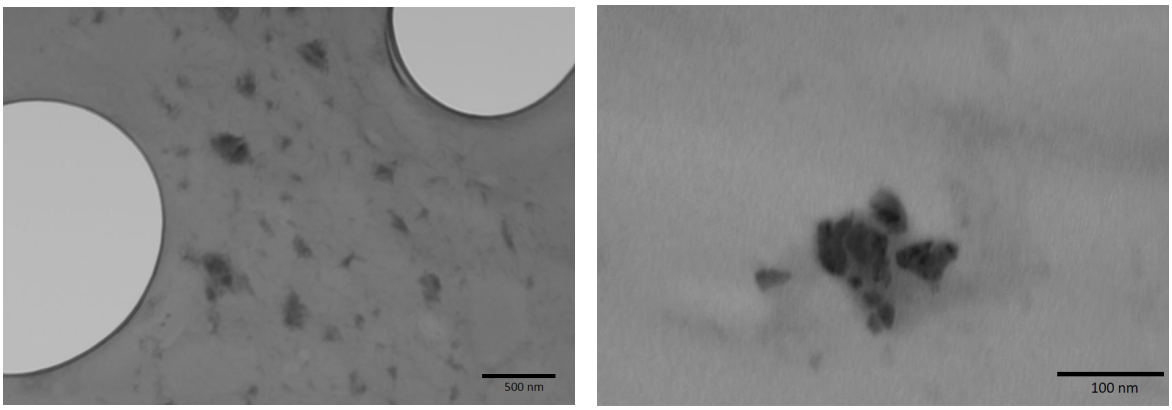

(a) (b)

Figure C.2: (a) Low magnification image which shows the dispersion of agglomerates in the EMHA3 epoxy nanocomposite, and (b) agglomerates which have formed in the EMHA1 epoxy nanocomposite.

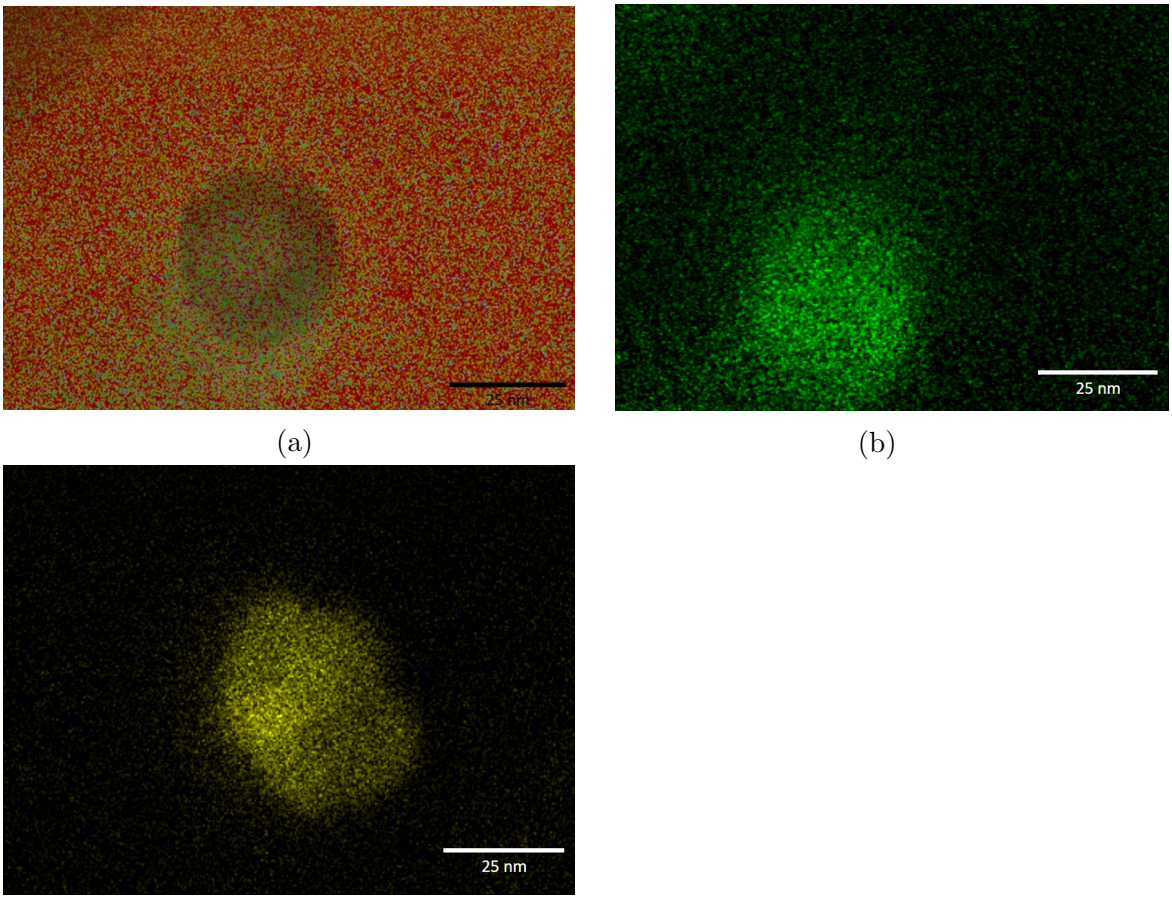

(a) (b)

(c)

Figure C.3: (a) Layered EDS image of the EMHA1-APTES epoxy nanocomposite. The red color represents the element C (carbon) and light green represents Al (aluminium), (b) EDS Al map of the EMHA1-APTES epoxy nanocomposite, (c) EDS Ti map of the EMHT1-APTES epoxy nanocomposite.

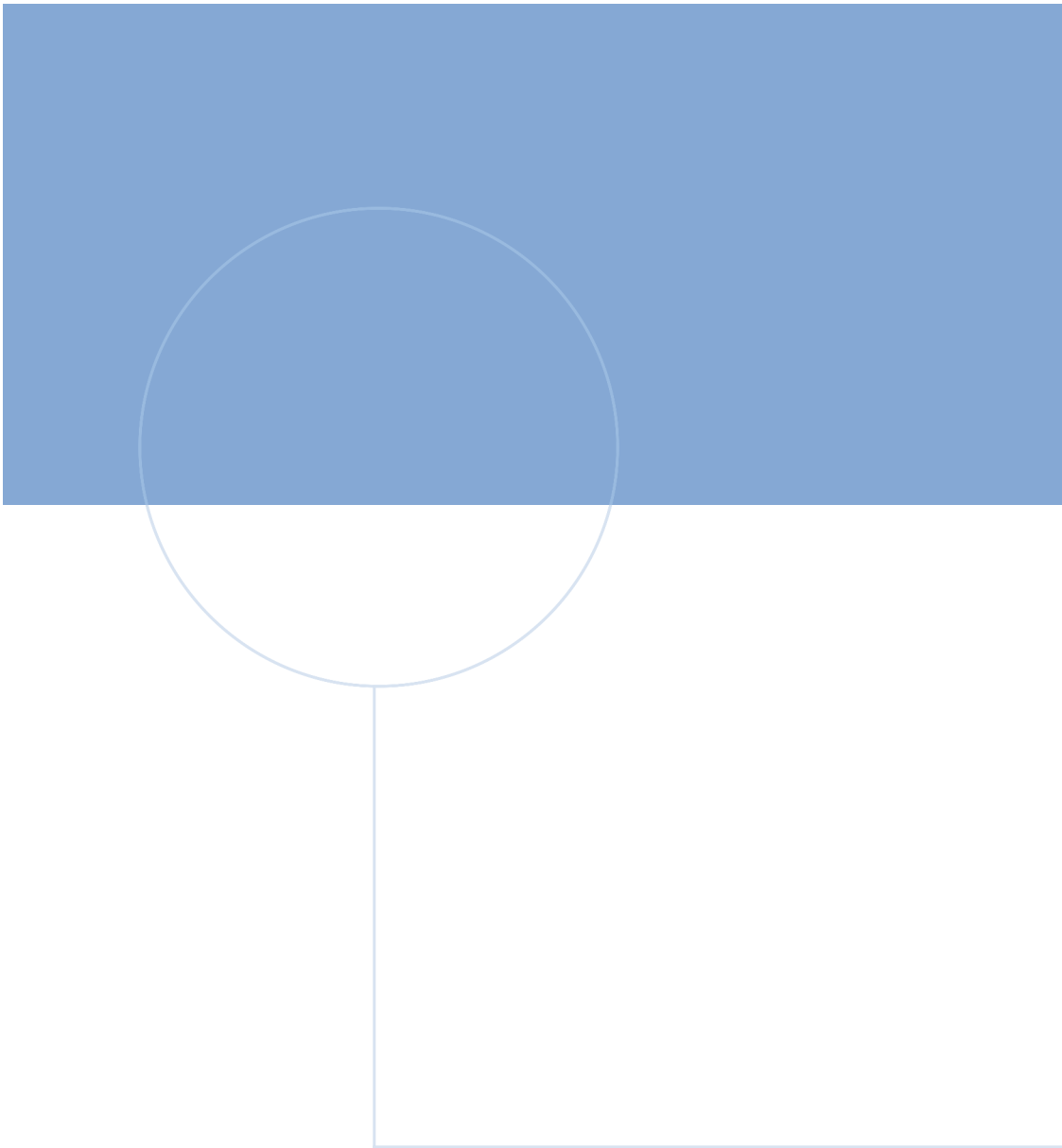

NTNU

Norwegian University of
Science and Technology